
Cosmic Microwave Background anisotropies: the power spectrum and beyond

Enrique Martínez-González

Instituto de Física de Cantabria, CSIC-Universidad de Cantabria, Avenida Los
Castros s/n, 39005 Santander, Spain martinez@ifca.unican.es

Most of the cosmological information extracted from the CMB has been obtained through the power spectrum, however there is much more to be learnt from the statistical distribution of the temperature random field. We review some recent developments in the study of the Cosmic Microwave Background (CMB) anisotropies and present a description of the novel tools developed to analyse the properties of the CMB anisotropies beyond the power spectrum.¹

1 Introduction

The standard scenario of the universe includes an early inflationary phase during which the universe experienced a drastic expansion. As a consequence of this inflationary period the homogeneity, isotropy and flatness of the universe that we observe today can be understood as a natural outcome, without a fine tuning of the initial conditions. Besides, quantum fluctuations of the fields dominating the dynamics at that early phase constitute the seeds which, after gravitational growing, will form the large scale structure (LSS) of the universe at the present time (for a detailed description of inflation and its consequences see e.g. [141]). The statistical distribution of the quantum fluctuations of the field responsible for inflation, known as inflaton, in the vacuum state is Gaussian. In addition, the energy density fluctuations generated from them are also Gaussian since they are related by linear theory. Moreover, the anisotropies

¹This review was almost complete before the second release of WMAP data which was made publicly available on March 2006. The major improvement has been made in the polarization data which are now much better understood regarding both systematics and foregrounds. This has implied a significant change in the value of the optical depth ($\tau \approx 0.09$). Another difference with respect to the values of the cosmological parameters estimated from the first year data is the possible significant deviation of the spectral index from unity as derived from the second release of data. Appart from these changes the rest of the parameters as well as the deviations from Gaussianity (“anomalies”) remain very much unaltered.

of the CMB are related to the energy density fluctuations by the linearized Einstein-Boltzmann equations, being therefore Gaussian distributed as well. This is a very important result since, for this particular statistical distribution, all the properties of the temperature random field are included in the second order moment. In harmonic space this is called the radiation power spectrum, usually denoted by C_ℓ .

The cosmological parameters which characterize the universe leave their imprint in the radiation power spectrum. In the standard inflationary scenario we only need to measure this second order moment to obtain all the possible information carried out by the CMB. This is in fact what many experiments have been doing with increasing precision in recent years. The BOOMERANG [64] and MAXIMA [91] experiments onboard stratospheric balloons were among the first to establish the spatial flatness of the universe. Most notably, the NASA Wilkinson Microwave Anisotropy Probe (WMAP) has measured the C_ℓ with high precision up to the multipole $\ell \approx 600$ [22]. This measurement has implied a high improvement in the determination of the cosmological parameters, reducing the uncertainties below 10% [220]. The uncertainties are further reduced when other cosmological data sets, like the LSS distribution of galaxies and SN Ia magnitude-redshift data, are combined with the CMB anisotropies [227]. Moreover, the degeneracy among some parameters present when only a single data set is considered is broken. This *concordance model* has been further confirmed by the first detection of polarization fluctuations by DASI [123] and the further determination of the polarization power spectra by WMAP [122], DASI [136], CBI [192] and BOOMERANG [168, 184]. An independent piece of evidence comes from the cross-correlation between CMB anisotropies and fluctuations in the galaxy number density. Several authors have found positive cross-correlations between the WMAP data and the NVSS radio galaxy survey [52], implying that the model of the universe is different from Einstein-de Sitter and, in the case of a flat universe, that the universe is dominated by a dark energy component [31, 78, 174, 8, 239, 161].

Measurements of the statistical distribution of the CMB temperature and polarization random field represent a unique probe of the early history of the universe. Thus, if the distribution is consistent with Gaussianity at a high precision then it would imply a nice confirmation of the standard inflationary model. On the contrary, if some significant deviations from normality are found then this result would contradict the standard single-field model and motivate the search for alternative scenarios of the early history of the universe. There have already been many suggestions of the latter in the past based on many different physical phenomena. Most notably, non-standard inflation models based on extensions of the standard one in many different ways -e.g. multi-field scenarios as the curvaton mechanism [145], inhomogeneous reheating scenario, etc (see [21] for a review)- and cosmic defects including global and local strings, monopoles, domain walls and textures [240].

The structure of the paper is as follows. In Sec. 2 we summarize the most relevant physical effects which generate the CMB temperature and polariza-

tion anisotropies. Sec. 3 deals with the constraints imposed by recent CMB data sets on the cosmological parameters as well as other cosmological data sets combined with the CMB. In Sec. 4 we describe the properties of the CMB anisotropies beyond the power spectrum and discuss possible sources of non-Gaussianity, inhomogeneity and anisotropy in their distribution on the celestial sphere. In Sec. 5 we discuss the methods developed for studies of the CMB temperature distribution and of its global isotropy whereas in Sec. 6 we review the analyses performed so far on CMB data sets measured by different experiments. Finally the conclusions are given in Sec. 7.

2 Theory

The CMB anisotropies are produced by different physical effects acting on this radiation before the last-scattering surface, when the universe was around 380000 years old. These *primary anisotropies* contain very valuable information on the early history of the universe and can be observed today almost unaffected. After the temperature of the photons drop below some 3000 degrees they are not able to ionize the hydrogen atoms and propagate freely. The physical effects producing the primary anisotropies at and after recombination can be summarised by the following equation [150, 204]:

$$\frac{\Delta T}{T}(\mathbf{n}) \approx \frac{\phi_e(\mathbf{n})}{3} + 2 \int_e^o \frac{\partial \phi}{\partial t} dt + \mathbf{n} \cdot (\mathbf{v}_o - \mathbf{v}_e) + \left(\frac{\Delta T}{T}(\mathbf{n}) \right)_e \quad (1)$$

The gravitational redshift suffered by the photons in their travel from the last scattering surface to the observer is given by the first two terms in the r.h.s. of eq. 1. They are known as *Sachs-Wolfe* and *late Integrated Sachs-Wolfe* effect, respectively [202]. The velocity of the baryon-photon fluid at recombination generates a Doppler effect. The intrinsic temperature of the photons at recombination, represented by the fourth term in the r.h.s. of eq. 1, also contributes to the total anisotropy. Eq. 1 accounts for the anisotropies at recombination. Before recombination, changes in the gravitational potential, due to the imperfect baryon-photon coupling, can also produce a gravitational redshift (the *early Integrated Sachs-Wolfe effect*). The accurate computation of all the contributions requires to solve the linearized coupled Einstein-Boltzmann equations. Several codes have been developed to numerically solve those equations as a function of the cosmological parameters (about 10, see below), being some of them publicly available (e.g. CMBFAST [213], CAMB [138]). A comparison among the results of different codes showed that the accuracy achieved is very good, reaching $\approx 0.1\%$ up to $\ell = 3000$ [212].

As will be explained below, a very relevant statistical quantity to compute is the 2-point correlation function of the temperature anisotropies or equivalently the correlation of the spherical harmonic coefficients:

$$\langle a_{\ell m} a_{\ell' m'}^* \rangle = C_{\ell} \delta_{\ell \ell'} \delta_{m m'}, \quad (2)$$

where C_ℓ is the anisotropy power spectrum and the $a_{\ell m}$ are the coefficients of the spherical harmonic expansion

$$\frac{\Delta T}{T}(\mathbf{n}) = \sum_{\ell, m} a_{\ell m} Y_{\ell m}(\mathbf{n}), \quad (3)$$

The homogeneity and isotropy of the universe have been assumed in eq. 2, i.e. the $a_{\ell m}$ are not correlated for different ℓ or m . In Fig. 1 the scales at which the different effects dominate the power spectrum C_ℓ are marked. As we can see, the gravitational effects dominate at the lower multipoles (large angular scales). At intermediate scales, $100 < \ell < 1000$, the spectrum is dominated by several oscillations, usually called *acoustic peaks*. These peaks appear as a consequence of the balance between the gravitational force and the radiation pressure. At the smallest scales, $\ell > 1000$, the C_ℓ are damped because of the width of recombination and the imperfections in the coupling of the photon-baryon fluid (*Silk effect*, [215]).

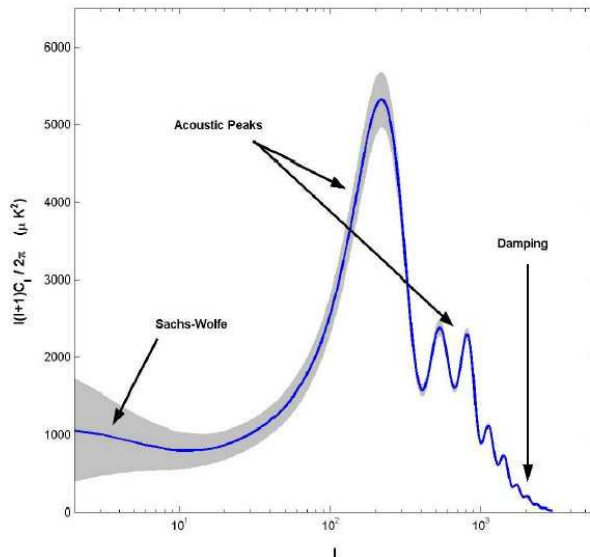


Fig. 1. CMB power spectrum C_ℓ for the best fit model given in [22]. The gray band represents the cosmic variance. The spectrum has been computed with the CMBFAST code [213].

When the small scales in the matter distribution become nonlinear and their collapse give rise to the formation of the first stars and quasars they start to reionize the surrounding matter. This ionized matter can interact again with the microwave photons and produce new anisotropies. *Secondary anisotropies* can be either produced by the scattering with free electrons or

by the gravitational effect of the matter density evolution. The scattering can leave a very clear imprint when the photons happen to cross the core of rich galaxy clusters where the electron density and temperature are very high (of several 10^{-3}cm^{-3} and $\sim 10^8\text{K}$, respectively). In this case the electrons inject energy to the photons through inverse Compton scattering, producing a distortion of the black-body spectrum. This effect is called *the Sunyaev-Zeldovich effect* [221].

The evolving gravitational wells in the large scale structure produce a gravitational redshift in the photons. This is known as the *late Integrated Sachs-Wolfe effect* [202] or *the Rees-Sciama effect* when the evolution is non-linear [200]. Besides, the trajectory of the photons is lensed by the same gravitational wells producing a noticeable effect on the CMB anisotropies at arcmin angular scales. One important issue in the observation of the CMB anisotropies is therefore to distinguish between primary and secondary anisotropies. In the case of the SZ effect, as the frequency dependence is different from the Planckian one, it is possible to separate the effect from the intrinsic CMB anisotropies by using multifrequency observations. However, for the lensing effect this is not possible and other properties, such as high-order correlations in the CMB temperature and polarization fields, have to be used (see e.g. [102, 84, 214]).

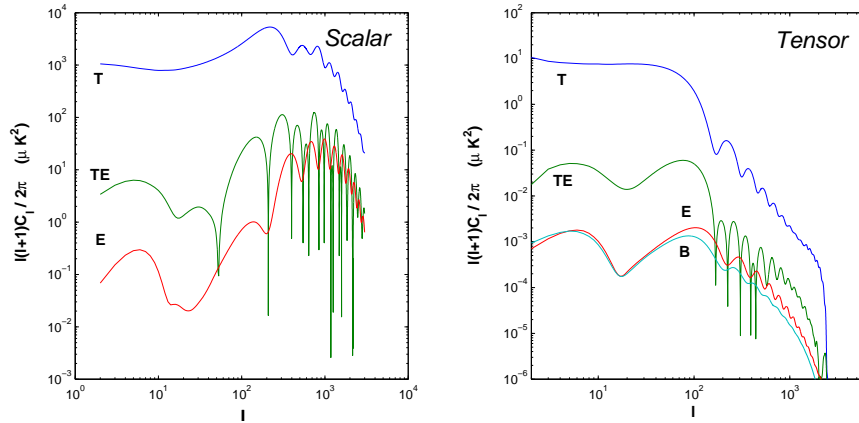


Fig. 2. Angular power spectra for temperature and polarization. The C_ℓ 's are plotted for scalar perturbations on the left and for tensor perturbations on the right, where a tensor/scalar ratio of $r = 0.01$ has been chosen. The rest of the parameters have been fixed to the best fit model of [22]. All the spectra have been computed with the CMBFAST code.

In the same manner that anisotropies in the temperature are expected in the gravitational instability scenario for structure formation, anisotropies in the polarization of the CMB are also expected. The physical effects giving rise to these anisotropies are, however, different. Linear polarization is generated

by Thompson scattering at the end of recombination when the growth of the mean free path of the photons allows temperature anisotropies to grow. In particular a quadrupole is formed in the reference frame of each electron producing polarization after the scattering (see, e.g., [47]). The expected level of polarization is however small $\approx 5\%$. As shown by [254, 113] two rotationally invariant quantities E, B can be constructed from the Stokes parameters Q, U . The different behaviour of E, B under parity transformations implies that only three spectra are needed to characterise CMB polarization: $C_\ell^E, C_\ell^B, C_\ell^{TE}$.

In addition to the anisotropies generated by physical effects associated to the energy-matter density perturbations (*scalar perturbations*), new anisotropies can be generated by a background of primordial gravitational waves (*tensor perturbations*). This background is also a generic prediction of inflation. The primordial power spectra for both scalar and tensor perturbations are usually characterised by a scale-free law of the form:

$$P_s(k) = A_s(k/k_0)^{n_s}, P_t(k) = A_t(k/k_0)^{n_t}, k_0 = 0.05 \text{ Mpc}^{-1}. \quad (4)$$

There is no observational evidence of the primordial background of gravitational waves yet. Upper limits have been imposed by the combination of WMAP and other high resolution CMB data with large scale structure data implying a tensor-to-scalar amplitude ratio $r \equiv A_t/A_s < 0.9$ [22], see next sections. In any case, the amplitude of both temperature and polarization power spectra produced by tensor perturbations are believed to be several orders of magnitude below the ones corresponding to the scalar perturbations. However, the B -mode can only be generated by gravitational waves and thus its detection represents a unique evidence of the existence of this primordial background. This is the reason why there is now so much interest in planning new more sensitive CMB experiments to detect polarization (see e.g. [30]). The detection of the B -mode is expected to be much harder than the already detected E -mode because of its intrinsically smaller amplitude and the relatively larger foreground emissions (expected from Galactic synchrotron and thermal dust and extragalactic radio sources; for a recent discussion of these issues see [230]). An additional complication comes from the lensing conversion of the E -mode to the B -mode [255] which is expected to dominate over the primordial B -mode at multipoles $\ell \gtrsim 100$ [119]. Several methods have been developed to reconstruct the gravitational lensing potential from the E and B -mode polarization correlations and remove the lensing contamination [105, 115, 211]. A more technical problem is the separation of the mixing of E and B -modes for observations with partial sky coverage for which other methods have been proposed [139, 36, 48].

Outside the inflationary scenario there are other possibilities to generate B -modes. For instance, cosmic strings or primordial magnetic fields would generate a vector and a vector plus tensor components of metric perturbations, respectively, contributing to the B -mode polarization (see e.g. [186, 140]). It is important to remark, however, that in the case of cosmic strings and other

topological defects their role as seeds for the large scale structure formation is already very much constrained by the observed C_ℓ , see below.

In Fig. 2 the different temperature and polarization power spectra corresponding to the primary anisotropies for the concordance model are plotted for the scalar and tensor perturbations assuming a value of $r = 0.01$. The power of the tensor perturbations is a few orders of magnitude below the corresponding scalar power spectra for $\ell \lesssim 100$ and decays strongly for larger multipoles.

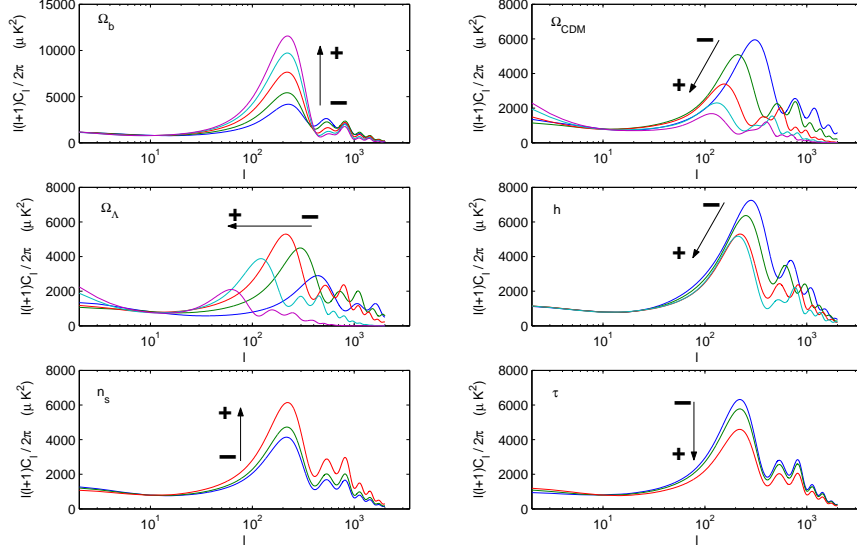


Fig. 3. Dependence of the temperature power spectrum C_ℓ on some relevant cosmological parameters (the spectra have been computed with the CMBFAST code).

Many parameters are needed to characterize the standar cosmological model. Their variation changes the amplitude and shape of the temperature and polarization power spectra in many different ways (see Fig. 3 for their effect on the temperature power spectrum). The cosmological parameters can be classified depending on whether they characterize the background universe or the primordial power spectrum.

The background Friedmann-Robertson-Walker universe and its matter and energy content are determined by the following parameters: *physical baryonic density*, $w_b = \Omega_b h^2$; *physical matter density*, $w_m = \Omega_m h^2$, where Ω_m is the matter density parameter including the contributions from baryons, cold dark matter and neutrinos, $\Omega_m = \Omega_b + \Omega_{CDM} + \Omega_\nu$; *physical neutrino density*, $w_\nu = \Omega_\nu h^2$; *dark energy equation of state parameter*, $w \equiv p_{DE}/\rho_{DE}$; *dark energy density*, Ω_{DE} (in case $w = -1$ the dark energy takes the form of a cosmological constant and its energy contribution is denoted by Ω_Λ) and the

Hubble constant, $h \equiv H_0/100 \text{ km s}^{-1} \text{ Mpc}^{-1}$.

The scalar and tensor primordial power spectra are characterized by the following parameters: *amplitude of the primordial scalar power spectrum*, A_s , defined by $P_s(k) = A_s(k/k_0)^{n_s}$, where $k_0 = 0.05 \text{ Mpc}^{-1}$; *scalar spectral index*, n_s ; *running index*, $\alpha = dn_s/d \ln k$, normally determined at the scale $k_0 = 0.05 \text{ Mpc}^{-1}$; *tensor-to-scalar ratio*, $r = A_t/A_s$; *tensor spectral index*, n_t , which is normally assumed to be $n_t = -r/8$ from the consistency relation of inflation (see e.g. [141]).

There is an extra parameter that accounts for the reionization history of the universe: *the optical depth*, $\tau = \sigma_T \int_{t_r}^{t_0} n_e(t) dt$, where σ_T is the Thompson cross-section and $n_e(t)$ is the electron number density as a function of time.

Besides, there are two possible types of matter density fluctuations: *adiabatic* which preserve the entropy per particle and *isocurvature* which preserve the total energy density. The standard inflationary scenario predicts fluctuations of the adiabatic type.

It is important to note that the manner in which some of the parameters enter in the calculation of the C_ℓ produce degeneracies. In particular, there is the well known geometrical degeneracy involving Ω_m , Ω_Λ and Ω_k , where Ω_k is the curvature density parameter, $\Omega_k \equiv 1 - \Omega_m - \Omega_\Lambda$ (an example of this degeneracy can be found in Fig. 5 of [155]). This fact makes clear the need to combine different cosmological data sets to break those degeneracies, as will be shown below.

3 Cosmological constraints

Several issues are important to bear in mind in the analysis of the CMB anisotropy data. First of all, the microwave sky is interpreted as a realization of the temperature anisotropy random field whose origin is in the inflationary era during the first moments in the history of the universe. The quantum fluctuations in the field dominating the dynamics at that epoch, called the inflaton field, generate energy perturbations which produce anisotropies in the CMB through the physical effects discussed in the previous section. The anisotropy field so generated is not ergodic on the sphere and so averages on the field do not coincide with averages on the sphere. This fact implies an intrinsic uncertainty in the statistical quantities extracted from the data, in particular in the power spectrum C_ℓ , called *the cosmic variance*. For the standard model this uncertainty is easy to compute since the random field is expected to be Gaussian, $\Delta C_\ell = C_\ell/\sqrt{\ell} + 0.5$ (this is valid for the whole sky, however when only a fraction of the sky f_{sky} is observed then the error is increased by approximately $f_{sky}^{-1/2}$). The value of this uncertainty is plotted in Fig. 1 for the standard model.

Second, at the millimeter wavelengths where the intensity of the black-body spectrum with temperature $\approx 2.725 \text{ K}$ is maximum there are other astronomical *foregrounds* which are also bright. These are the Galactic foregrounds:

synchrotron, free-free and thermal dust, and also the extragalactic sources whose emission peaks in the radio or the infrared bands. The problem of separating the foreground emission from the cosmic signal is crucial and requires multifrequency observations and a good understanding of the frequency and spatial properties of the foregrounds. In recent years a strong effort in this direction is being made by the CMB community, devising new instruments optimized to observe at frequencies around 100GHz where the CMB emission dominates over the foregrounds (for both temperature and polarization, see e.g. [230]), and developing sophisticated methods of component separation (see e.g. [67, 17] in this volume). In any case, there are still regions of the sky (near the Galactic plane and others dominated by extragalactic sources) where the CMB is unavoidably hampered by the foregrounds. These contaminated regions are usually masked and therefore removed from the data analyses.

In the next subsections we will discuss the results obtained on the model of the universe based on the C_ℓ . Following the standard model and some observational evidences, the anisotropies are assumed to be Gaussian and thus all the statistical information is included in the second-order moments. It is for this reason that most of the analyses performed to constrain the cosmological parameters are based on the C_ℓ . Even the likelihood methods to derive those parameters are based on the Gaussian assumption (see for instance the review by [104]). In Sec. 5 and after we will also review the works made to test the Gaussian assumption.

3.1 Cosmological parameters from the C_ℓ

In the last decade there has been a strong technological development in CMB devices allowing very sensitive measurements of the temperature of the microwave sky. Due to the atmospheric emission at microwave frequencies the experiments have to be located at very dry places on Earth or onboard of balloons or satellites. In particular the space mission NASA WMAP has made possible to cover the whole sky from a privileged position (the Lagrangian point 2 of the Sun-Earth system), saved from contaminating emissions coming from the Earth, Moon and Sun. In table 1 the values of the cosmological parameters determined with the first year data of that mission are shown. An interesting result that can be derived from this table is that the Einstein-de-Sitter model (i.e. flat geometry with null dark energy density) is many standard deviations away from the best fit model (assuming a flat universe and an optical depth $\tau < 0.3$) [220].

The resolution of the WMAP experiment allows a good precision in the determination of the C_ℓ up to multipoles $\ell \lesssim 600$. Other experiments based on the ground like ACBAR [128], CBI [191], VSA [69] and balloon-borne like BOOMERANG [112] are able to reach higher resolutions covering small patches on the sky with good sensitivity. The data obtained with these experiments therefore complement very well the WMAP ones. In Fig. 4 the temperature anisotropy results from WMAP and the other high resolution

Table 1. Cosmological parameters using only WMAP first year data. In the fit the universe is assumed to be spatially flat and the value of the optical depth is constrained to $\tau < 0.3$ (from [220]). The physical baryonic density parameter w_b is defined by $w_b = \Omega_b h^2$ and similarly for the physical matter density w_m which includes the contribution from all the matter species: baryons, cold dark matter (CDM) and neutrinos.

<i>Parameter Values (68% CL)</i>	
w_b	0.024 ± 0.001
w_m	0.14 ± 0.02
h	0.72 ± 0.05
A_s	0.9 ± 0.1
τ	$0.166^{+0.076}_{-0.071}$
n_s	0.99 ± 0.04

experiments as a function of the multipole are shown. We can see that the concordance model follows quite well the data up to $\ell \approx 2000$. For higher multipoles only ACBAR and CBI experiments have enough resolution and the data seem to indicate an excess of power as compared to the model prediction. This excess can be interpreted as a contribution from secondary anisotropies coming from the SZ effect [28] or/and the emission of radio sources [231]. However, new multifrequency data at arcminutes resolution are necessary to confirm the excess and discriminate among possible causes.

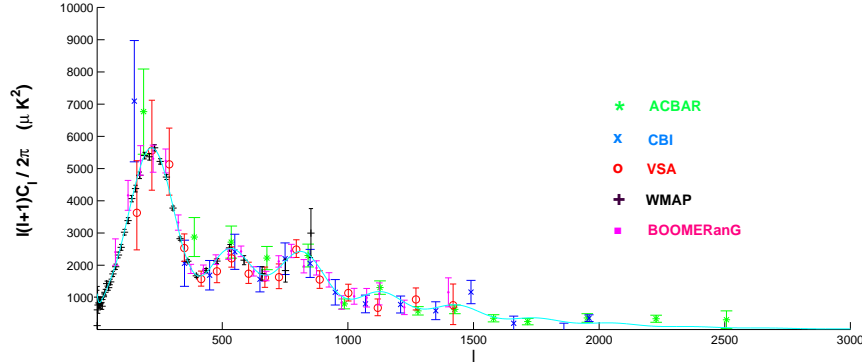


Fig. 4. The temperature power spectrum C_ℓ measured by WMAP, ACBAR, CBI, VSA and BOOMERANG, compared to the best fit model given by [22].

Since the recent detection of polarization by the DASI experiment [123] several experiments have measured the TE cross-power spectrum C_ℓ^{TE} (WMAP [122], CBI [192] and BOOMERANG [184]) and the EE one C_ℓ^E (CBI [192] and BOOMERANG [168]). The sensitivity of the polarization data is not yet

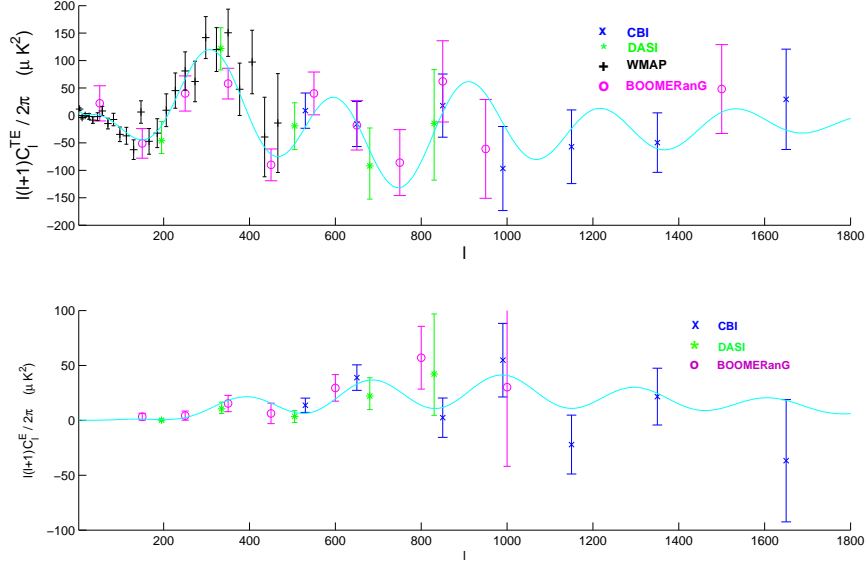


Fig. 5. Polarization power spectra measured by DASI, WMAP, CBI and BOOMERANG (TE) and DASI, CBI and BOOMERANG (E). Also plotted is the best fit model given by [22].

comparable to the temperature one. However, it is already sufficient to confirm the main features of the concordance model and, more specifically, the adiabatic nature of the primordial matter density fluctuations. Namely, that the peaks of the polarization power spectrum, C_ℓ^E , are out of phase with the temperature C_ℓ ones. The TE cross-power spectrum, C_ℓ^{TE} , and the E -mode polarization power spectrum, C_ℓ^E , are shown in Fig. 5.

The next challenge is the detection of the B -mode polarization. As commented in the previous section this detection would unambiguously indicate the existence of a background of primordial gravitational waves. Moreover, it is the only chance that we have to know about its possible existence in the next decade since experiments aimed to directly detect gravitational waves are still not sensitive enough. The amplitude of this background, A_t , or equivalently the tensor-to-scalar ratio r , is proportional to the energy scale of inflation. Whereas the all-sky ESA Planck space mission² [185] will be limited by instrument sensitivity, being able to detect values down to $r \approx 0.05$ [230], planned very sensitive ground-based experiments covering small patches of the sky and carrying arrays of 1000's of detectors like PolarBear [187], Clover[146], BRAIN [156] or QUIET [189], are expected to be limited by the ability to remove the foregrounds and are expected to reach values of $r \approx 0.01$ in the best case. In order to significantly improve this limit we will have to wait for

²<http://www.rssd.esa.int/Planck>

the next generation of space missions with $10^3 - 10^4$ detectors, now under discussion by ESA, NASA and other space agencies [246, 30]. The combination of complete sky coverage, very sensitive multifrequency observations and an optimal control of systematics make the space missions the ultimate experiments to go down to values $r \sim 10^{-3} - 10^{-4}$ allowing to probe energy scales for inflation down to $\approx 5 \times 10^{15} \text{ GeV}$ [230].

3.2 Combination with other cosmological data sets

The first observations showing the existence of a dark energy dominating the dynamics of the universe were those based on the *luminosity distance-redshift diagram* determined with supernovae SN Ia [194, 182]. Those results were, however, taken with certain caution because of the assumption made that the low and high redshift SN Ia had the same light curve behaviour (in addition, there were many other possible systematics which raised some concern). In any case, SN Ia data complements very well the CMB anisotropies since for the former the dependence of the model prediction on the dark matter and dark energy density parameters enters approximately as $\Omega_m - \Omega_\Lambda$, and as $\Omega_m + \Omega_\Lambda$ for the latter (see Fig. 6).

The large galaxy surveys, *2-degree Field Galaxy Redshift Survey* 2dFGRS [181] and *Sloan Digital Sky Survey* SDSS [226] have recently reached ≈ 200000 measured redshifts on large fractions of the sky. A three-dimensional power spectrum $P(k)$ of density perturbations is estimated with each data set. The cosmological parameters enter in the prediction of $P(k)$ through the initial power spectrum (A_s, n_s) and the transfer function which linearly connects the initial and present spectra. Besides, an additional parameter, *the bias* b , is required to link the galaxy power spectrum to the matter one $P(k)$. Although this parameter will in principle depend on the scale, however, it is found that at large scales b is scale-independent (see e.g. [227]). There are still other problematics that need to be corrected before using the data for accurate parameter determination such as the redshift-space distortions due to galaxy peculiar velocities, survey geometry effects, ... Once those effects are corrected the galaxy redshift surveys play a key role in breaking the CMB degeneracies. For instance, the degeneracies of the model predictions on both data sets on the plane formed by the spectral shape parameter $h\Omega_m$ and the baryon fraction Ω_b/Ω_m are almost orthogonal.

Results on 11 free cosmological parameters combining CMB data (WMAP [99], CBI [191], ACBAR [128]) with the 2dFGRS galaxy redshift survey [181] are given in table 2. As can be seen from that table, the combination of different cosmological data sets has allowed for the first time an accuracy $\lesssim 10\%$ in the determination of most parameters. Results combining WMAP data with the SDSS galaxy redshift survey [226] have also produced similar values for the parameters [227].

In addition to CMB and galaxy surveys, other combinations including the

Table 2. Cosmological parameters from WMAP, CBI, ACBAR and 2dFGRS combined data (from [22]).

<i>Parameter</i>	<i>Values (68% CL)</i>
w_b	0.0224 ± 0.0009
w_m	$0.135^{+0.008}_{-0.009}$
w_ν	< 0.0076 (95% CL)
w	< -0.78 (95% CL)
Ω_{DE}	0.73 ± 0.04
h	$0.71^{+0.04}_{-0.03}$
τ	0.17 ± 0.04
A_s	$0.833^{+0.086}_{-0.083}$
n_s	0.93 ± 0.03
α	$-0.031^{+0.016}_{-0.018}$
r	< 0.90 (95% CL)

HST key project value for the Hubble parameter [81], SN Ia magnitude-redshift data [195, 229], Ly α forest power spectrum [60, 159] or abundancies of reach clusters of galaxies can help to improve the results [220, 210, 190, 110]. Confidence contours in the plane $(\Omega_m, \Omega_\Lambda)$ for the combination CMB+SN Ia+cluster abundancies are given in Fig. 6. The complementarity of the three data sets to break degeneracies is clearly shown. A similar effect in the plane (Ω_m, w) is obtained by combining CMB+2dFGRS+SN Ia (see Fig. 7).

Recently, an independent piece of evidence that the universe is not Einstein-de Sitter (flat geometry with null dark energy density) has been found by cross-correlating the CMB map with galaxy survey maps. The same evolving gravitational potential wells which generate the large scale structure of the galaxy distribution also produce the gravitational redshift in the CMB photons at late times (the *late ISW* effect, see Sec. 2). The amplitude and sign of the cross-correlation depends on three parameters Ω_{DE} , Ω_k and h . For a flat universe, as indicated by many different observations as discussed above, a positive signal will unambiguously imply the presence of dark energy. This is the case found recently cross-correlating the WMAP map with different large scale structure surveys (the radio source survey NVSS [52], the X-ray survey HEAO-1 [26], the optical SDSS [1], the near-infrared survey 2MASS [216]) [31, 78, 174, 8, 239]. In [239] three different methods were used to estimate the *WMAP-NVSS cross-correlation*: direct temperature anisotropy-galaxy number density, cross-power spectrum and covariance wavelet coefficients. A clear positive signal was found in the three cases using a maximum likelihood analysis. The significance of a non-null dark energy reaches 3.5σ for the cross-power spectrum. This is also the maximum significance detection of the ISW effect up to date (see also [161] for a recent analysis using directional wavelets). The reason for the different detection levels obtained with the three methods lies in the incomplete sky coverage available for the analysis. Otherwise, for a whole

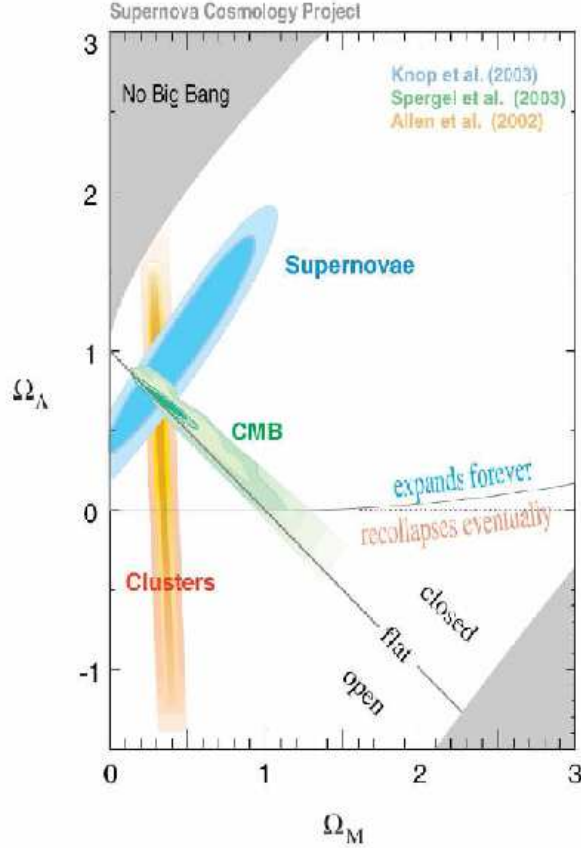


Fig. 6. Confidence contours for the pair $(\Omega_m, \Omega_\Lambda)$ combining SN Ia, CMB and cluster density data (taken from the Supernova Cosmology Project).

sky coverage the same detection level will be guaranteed by the maximum likelihood method since the likelihood is invariant under linear transformations of the data. In Fig. 8 we plot the two maps together with the combined mask needed to avoid the regions contaminated by foregrounds in the WMAP map and unobserved regions of the NVSS survey. An analysis allowing variations in the dark energy equation of state parameter w also shows a preferred value close to -1 . The 2D confidence contours for the pair Ω_{DE}, w and the marginalized likelihoods are plotted in Fig. 9

3.3 Summary of the main results

From the previous discussion about the cosmological implications of the large amounts of data already collected on the CMB anisotropies, galaxy redshift

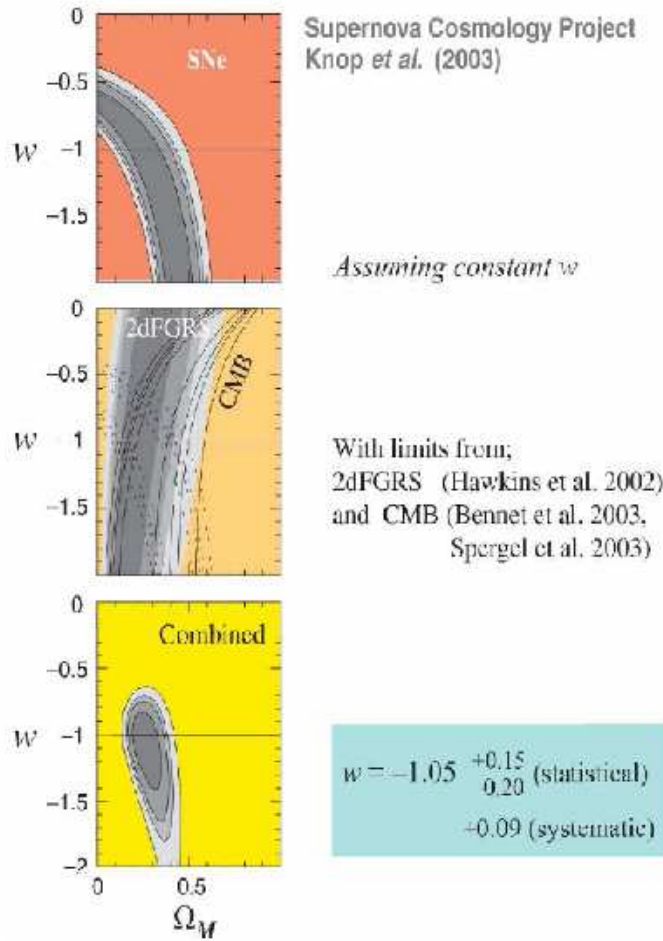


Fig. 7. Confidence contours for the pair (Ω_m, w) using either SN Ia, 2dFGRS and CMB or a combination of the three data sets (taken from the Supernova Cosmology Project).

surveys, etc, the most important result is the convergence of all those cosmological data sets towards the same model of the universe, *the concordance model*. Below we summarize the main characteristics of this model and other consequences implied by the data:

- The geometry of the universe is very close to flat.
- The dynamics is dominated by a dark energy whose equation of state is almost that of a cosmological constant.
- Most of the matter content is in the form of cold dark matter.

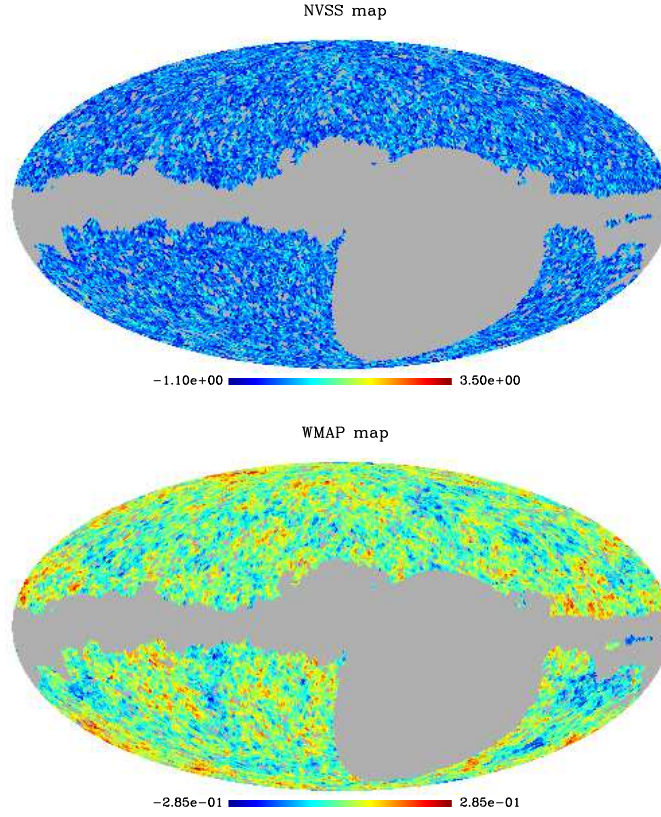


Fig. 8. The radio sources NVSS and the combined WMAP maps including the common masks used in the cross-correlation analyses (taken from [239]).

- The large scale structure of the universe was seeded by quantum fluctuations in the very early universe that evolved via gravitational instability (the first evidence of this came from COBE-DMR [219]).
- The initial matter-energy density fluctuations were of the adiabatic type.
- Topological defects did not play a dominant role in the structure formation of the universe.
- Primordial gravitational waves do not appreciably contribute to neither the temperature nor the E-mode polarization anisotropies (up to the present sensitivities reached).
- The reionization happened at relatively early times, $z \gtrsim 10$.³
- The initial fluctuations were close to a homogeneous and isotropic Gaussian random field (see however the next sections).

³Considering the second release of WMAP data, z is indeed around 10.

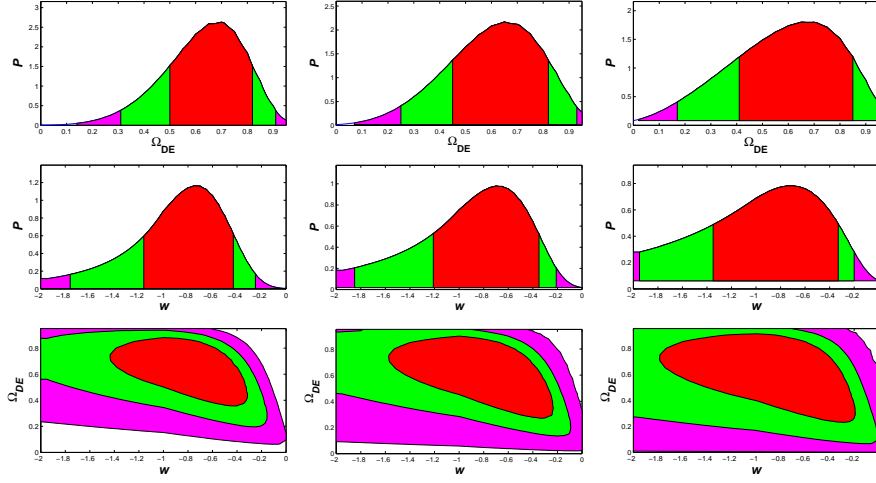


Fig. 9. The marginalized pdf for Ω_{DE} (upper) and w (middle). Contours of the 2D likelihood are given in the lower pannel (taken from [239]). From left to right the three columns correspond to the results obtained with the WMAP-NVSS cross-power spectrum, covariance wavelet coefficients and temperature anisotropy–galaxy number density cross-correlation, respectively.

4 Beyond the power spectrum: sources of non-Gaussianity

As it was said before, single-field inflationary models predict Gaussian temperature fluctuations homogeneously and isotropically distributed on the sphere. In this case all the information is contained in the power spectrum or, equivalently, the two-point correlation function. In the previous sections all the discussion has been based on such statistical quantity. However, this picture can be modified if the origin of the primordial fluctuations is different (e.g., the presence of topological defects or non-standard inflation). If this is the case, the generated fluctuations will show non-Gaussian features (e.g., non-random phases) and the statistical information is not only contained in the second order moment. Even if the primordial fluctuations generated in the early universe are Gaussian, non-Gaussianities can appear after recombination when the non-linear matter density evolution takes place and new anisotropies are generated. These secondary anisotropies, as already discussed in Sec. sec:theory, can be produced by the gravitational lensing effect, the interaction of CMB photons with reionised matter or the gravitational effect of the non-linear evolution of the large scale structure. On the other hand, the universe is believed to be a Friedmann-Robertson-Walker (FRW) model with a simply-connected topology. Departures from this scenario, either its geometry or/and topology, will induce inhomogeneity or/and anisotropy in the statistical nature of the temperature distribution on the sphere (e.g. hot

spots, rings, multiple images). Systematics arising from instruments and data processing as well as residues left after foreground removal to get the intrinsic CMB signal will inevitably introduce artefacts which will contaminate the primordial signal. It is therefore crucial to disentangle these artifacts from primary and secondary non-Gaussianity (see [18] for a recent study of the residues left by different component separation methods).

4.1 Models of the early universe

Even in the standard inflationary scenario small deviations from normality can appear as a consequence of second-order effects during the evolution of density fluctuations after inflation finishes (see [21] for a detailed discussion). The non-Gaussianity produced by those second-order effects must be therefore present in any inflationary model. In the case of non-standard inflation, as the curvaton scenario or inhomogeneous reheating, the primordial non-Gaussianity should be added to that term. The level of non-Gaussianity in the cosmological perturbations can be phenomenologically characterized by the *non-linear parameter* f_{NL} in the gravitational potential:

$$\Phi = \Phi_L + f_{NL}\Phi_L^2, \quad (5)$$

where Φ_L is the gravitational potential at linear order. Although f_{NL} will in general depend on the scale, from a practical data analysis point of view it is useful to consider it as a constant [21]. Recently, a complete second-order calculation has allowed an estimate of an effective f_{NL}^{eff} for some inflationary scenarios and considering only a limited number of multipoles $\ell_{max} \leq 500$ due to computational cost [142]. The result is a value $f_{NL}^{eff}(\ell_{max}) \simeq 4$ with an increasing trend towards higher multipoles. This level of non-Gaussianity might be marginally detected with future experiments like Planck.

Topological defects in the universe are expected to appear as a natural consequence of phase transitions in the early universe (for a detailed description see [240]). They are associated to symmetry breaking of fields responsible for the different particle interactions. According to their dimensionality they can be classified in the following types: monopoles, cosmic strings, domain walls and textures. We already know from the mismatch between the observed oscillations of the C_ℓ and the generic featureless spectra predicted by cosmic defects that their role in the generation of the cosmological fluctuations has to be sub-dominant. The contribution of both global and local defects to the C_ℓ is constrained to be $\lesssim 10 - 20\%$ [24, 79, 133, 252, 251]. However, their intrinsically active role in seeding structure formation in the universe produces a characteristic non-Gaussian CMB temperature field. On large angular scales the superposition of many defects tends to Gaussianity by the central limit theorem. On scales smaller than the projected inter-defect separation non-Gaussianity can be seen as line-like discontinuities, in the case of strings, and as hot/cold spots in the case of monopoles and textures. Cosmic strings, the

best studied defects, have recently received renewed attention because they are produced in a wide class of string theory models where inflation arises from the collisions of branes.

4.2 Geometry and topology

The angular distribution of the CMB temperature and polarization fluctuations on the sky is very sensitive to the spacetime metric of the universe. On the largest scales it is assumed that the metric corresponds to the Friedmann-Robertson-Walker one. Deviations from this metric, even if small, can lead to noticeable signatures in the CMB anisotropy. In particular for homogeneous and anisotropic models (classified as Bianchi models), it is well known that global shear or rotation can produce a spiral pattern or hot spots on the CMB sky [19, 108]. Since those signatures are on large angular scales, strong limits on those models were already derived from the COBE-DMR experiment [121, 152, 35]. More recently, asymmetries/non-Gaussianities found in the WMAP first-year data have been nicely fitted with a Bianchi VII_h model [108]. However, even considering extensions of the Bianchi VII_h models in which a Ω_Λ term is included, the values of the parameters which fit the large scale asymmetries are ruled out by current observations at high significance [109, 32].

Due to the local character of the General Theory of Relativity the global topology of the universe is not theoretically constrained (for different topologies discussed in the literature see e.g. [129, 244, 235, 137]). Non-trivial topologies leave imprints in the CMB anisotropy at large angular scales which can be observed as anisotropic patterns, matched circles or, more generically, deviations from a Gaussian random field (see e.g. [58, 106, 197]). The observability of those signatures depends on the topology scale as compared to the horizon scale [206]. Detailed CMB simulations in non-trivial topologies are required to extract the maximum information from the data (see [193, 100]). Precision all-sky surveys are necessary to obtain strong limits on global topology. The COBE-DMR data already constrained several topological models (see e.g. [65, 198, 197]). More recently, the WMAP data were also analysed to further constrain topology finding no evidence of non-trivial topologies [127, 59]. Moreover, theoretical limits are derived for the size of the topologies that can be detected [127]. Besides, [144, 199, 11] have claimed a dodecahedral topology for the universe to explain the anomalies found at the lowest multipoles of the WMAP data. The next all-sky experiment, the Planck mission, will obtain more sensitive data in a wider frequency range allowing a better separation of the CMB from Galactic emissions and therefore a better determination of the low-order multipoles. It will thus help to clarify the present situation and to determine whether the present anomalies are due to systematics, foreground residues or are indeed true anisotropies of the CMB.

4.3 Secondary Anisotropies

As already commented in Sec. 2, the temperature anisotropies of the CMB are usually divided in primary and secondary. The former are generated prior to recombination and are directly related to the initial density fluctuations. The latter are generated after matter-radiation decoupling and arise from the interaction of the CMB photons with the matter. These interactions can be of gravitational type (e.g., *Rees-Sciama* effect, [200, 150]), or of scattering type when the matter is ionised (e.g., *Sunyaev-Zel'dovich (SZ)* effect of galaxy clusters [221] or *Ostriker-Vishniac* effect for a homogeneous re-ionisation [176, 241] or, on the contrary, *inhomogeneous re-ionisation* of the universe [3, 88, 118]). Secondary fluctuations will in general induce non-Gaussian signatures that will add to the intrinsic statistical properties of the CMB anisotropies. Their contributions to the bispectrum (third order moment in harmonic space, see next section) during reionization have been studied in [54]. More recently, it has been shown that the imprint of the Ostriker-Vishniac effect can be characterized by an undetectable bispectrum and a significant trispectrum (fourth order moment in harmonic space) [40]. The Rees-Sciama effect due to non-linear evolution of matter is expected to produce three-point correlations much below the cosmic variance [164].

The SZ effect due to galaxy clusters is one of the most important sources of secondary anisotropies. Two types of SZ effect can be distinguished: the *thermal* effect, induced by the CMB photon scattering off free electrons in the hot intra-cluster gas, and the *kinetic SZ* effect due to Doppler shift of the photons when the clusters move with respect to the CMB rest frame. Owing to its peculiar spectral signature the thermal effect will be separated to a good accuracy and thus removed from the cosmological signal. However, the contribution from kinetic SZ effect, which is spectrally indistinguishable from the primary anisotropies, will not be easily subtracted, and will thus remain a potentially significant non-Gaussian foreground contribution. The SZ effect of galaxy clusters is by nature a non-Gaussian process. Several studies have aimed at characterising the non-Gaussian signature, either in wavelet space (see e.g. [4]) or in the real one ([55, 253]), in order to address its detectability and extract the maximum information from it.

On its way from the last-scattering surface to us, the CMB radiation passes mass inhomogeneities which deflect its paths by the gravitational lensing effect. This process can approximately be described as a random walk of light through a continuous field of mass inhomogeneities, and thus leads to a diffusion process. The diffusion tends to broaden structures in the CMB on angular scales smaller than $\sim 10'$ (see [20] for a review).

As long as the density inhomogeneities can be described as a Gaussian random field, the light is slightly deflected and its distribution is a Gaussian random process. A purely Gaussian CMB would therefore remain approximately Gaussian despite the deflection at least for $l \lesssim 1000$. However, at smaller scales non-Gaussianity is imposed on an originally Gaussian CMB

by producing correlations between temperature fluctuations at large scales (through the *late ISW* effect) and light deflections which generate noticeable effects at several arcmin resolution [102, 84, 214]. Those correlations induce high-order correlations in the CMB temperature and polarization fields. In particular, a bispectrum is generated whose signal to cosmic variance noise is higher for polarization and polarization-temperature bispectra than for those involving the temperature alone [102].

Gravitational lensing by galaxy clusters can also lead to non-Gaussian features in the CMB through their strong lensing effect. While their origin is not physically distinct from lensing by large-scale structures, galaxy clusters can be individually identified through their thermal Sunyaev-Zel'dovich effect and, for the brightest cases, extracted from CMB maps. Methods to remove non-Gaussianity from CMB maps therefore have to distinguish between lensing by clusters and by large-scale structures.

5 Methods to detect and characterize deviations from Gaussianity, standard geometry and trivial topology

There are infinite ways in which a random field can departure from Gaussianity. For instance, the cumulants above order 2 should be zero for a Gaussian distribution and thus a non-null value taken by any of them would represent a deviation from normality. In Fig. 10 it is shown a Gaussian map corresponding to the concordance model together with other non-Gaussian ones with the same power spectrum but with small amounts of skewness or kurtosis. Hence, there is not a unique way to detect and characterize deviations from Gaussianity. Depending on the kind of features that are investigated some specific methods will prove to be more efficient than others. A variety of methods have been already proposed to search for non-Gaussianity in the temperature or polarization maps. Acting in different spaces (real, harmonic, wavelet, eigenmode, ...) they are able to extract relevant information which is otherwise hidden in the fluctuation maps. Improved methods for the combined temperature and polarization maps are expected to be developed in the coming years motivated by the large amounts of new data expected to be collected by the new experiments (specially the all-sky WMAP and Planck satellites).

An important difference among the methods is whether they are guided or blind. The former are intended to test specific models of non-Gaussianity. The latter do not assume any form of non-Gaussianity. Guided methods would be more powerful in constraining non-Gaussianity than the blind ones at the cost of being model-dependent. Both methods have been used in the literature with different results: while guided methods have imposed upper limits on the non-linear parameter f_{NL} some blind methods have obtained significant deviations of Gaussianity (see Sec. 6.2).

Below we summarize different methods which can be used to detect and characterize non-Gaussianity in temperature/polarization maps.

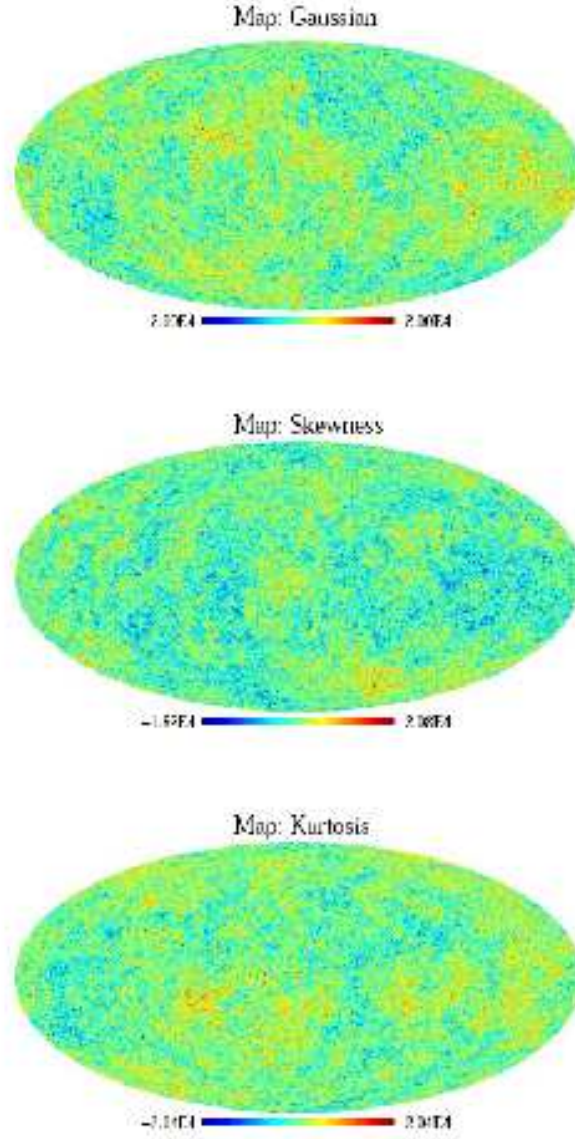


Fig. 10. Map simulations for Planck LFI 33 GHz ($N_{\text{side}} = 256$, FWHM = 33 arcmin). Non-Gaussian features have been introduced in the map using the Edgeworth expansion (from [153]).

Methods based on *real space* are very useful for picking out statistical features. However, they may be insensitive to any localized features. Standard statistics like *moments* and *cumulants*, obtained from the moment generating function and its logarithm or cumulant generating function, are included in the 1-point probability distribution function (pdf). Any non-zero amplitude for any cumulant of order higher than 2 would be an indication of the presence of non-Gaussianity. It is more common to use the skewness and kurtosis, the third and fourth standardized moments, which are defined by the ratio of the 3 and 4-order cumulants normalized to the square root of the 2-order cumulant to the power of the corresponding order, respectively. All the statistical information is, however, included in the n-point pdf. For the Gaussian case, it is sufficient to specify the 2-point correlations. Any positive detection of reduced correlations above order 2 would imply deviations from Gaussianity in the data. Tests of normality based on the *Edgeworth expansion* for estimating the skewness of the COBE maps have been developed by [53]. The Edgeworth expansion allows to describe perturbations of the Gaussian distribution in terms of a series of cumulants (see [114]). An alternative expansion derived from the Hilbert space of a linear harmonic oscillator, producing a proper normalized distribution under any truncation, has been proposed by [196]. Other approaches based on *goodness-of-fit tests* of normality have recently been developed and applied to the MAXIMA data [42].

A different approach to test Gaussianity is based on *scalar quantities* on the sphere. These quantities are constructed with the first and second covariant derivatives of the temperature field. A well known example is the local curvature (see [72, 93]) but many others can be defined as the modulus of the gradient, shape index, determinant of the Hessian matrix, ... (see [166] for a detailed study of those quantities). These scalar quantities have been recently shown to be good detectors of small deviations from Gaussianity as given by the Edgeworth expansion [167]. Analyses based on *statistics of extrema* and *excursion sets* (e.g., number, correlations, eccentricities) provide very robust results since extrema are often many sigmas above the noise level. Those quantities can be computed (semi-)analytically for a Gaussian field as was shown in the pioneering work [27]. Also, it has been shown that the *Gaussian curvature* of peaks is an efficient discriminator of non-Gaussianity [16]. The *extrema correlation function* for a Gaussian field is accurately computed in [96, 97] whereas [13] computed the *correlation of excursion sets* for Gaussian and some non-Gaussian temperature distributions. *Minkowski functionals* describe the morphology of the excursion sets which are defined by thresholding the temperature field. They are three for the 2D sphere: total contour of the excursion set, total area and the total curvature (or the genus). Analytical expressions can be obtained for the Gaussian field. These morphological descriptors have been implemented on the HEALPix pixelisation [85] of the sphere by [242].

Alternative methods based on *multifractal analysis* and *surface roughness*, widely used in many branches of physics, have also been proposed to detect non-Gaussianity in CMB maps [70, 165].

Spherical harmonics space statistics are attractive as the predictions for Gaussian fields can in some cases be computed analytically, and their covariance properties may also be computed in principle. In practice, we may not be able to benefit from these advantages due to the complexities and size of the experimental data sets. As for the other statistics, sensitivity to artefacts such as those arising from the observing strategy and, in particular, incomplete foreground subtraction, need to be assessed. The *bispectrum*, $B_{\ell_1 \ell_2 \ell_3}$, is the rotationally invariant third-order moment of spherical harmonic coefficients and has been very often used to test different data sets. It is given by the following expression (see [103, 21] for a derivation of this and higher order moments):

$$B_{\ell_1 \ell_2 \ell_3} = \sum_{m_1 m_2 m_3} \begin{pmatrix} \ell_1 & \ell_2 & \ell_3 \\ m_1 & m_2 & m_3 \end{pmatrix} a_{\ell_1 m_1} a_{\ell_2 m_2} a_{\ell_3 m_3}, \quad (6)$$

where (...) is the Wigner-3j symbol. The bispectrum must satisfy the selection rules, requiring that $\ell_1 + \ell_2 + \ell_3$ be even, the triangular rule $|\ell_1 - \ell_2| \leq \ell_3 \leq \ell_1 + \ell_2$ and that $m_3 = m_1 + m_2$. For simplicity reasons often the case that all multipoles are equal, $\ell_1 = \ell_2 = \ell_3$, has been considered (see e.g. [77] for an application to COBE-DMR). Inter-scale correlations of the form $B_{\ell-1 \ell \ell+1}$ have also been used (e.g. [147]). They are generically expected in models with scaling seeds like cosmic defects. Other components with more distant multipoles may be considered but they are often dominated by noise. A fast algorithm to compute the bispectrum from HEALPix-formatted data has been developed by [124] and applied to the HEALPix-formatted COBE-DMR data. [126] have recently implemented an algorithm to compute the *trispectrum* (fourth order moment in harmonic space) in the HEALPix pixelization and have applied it to the COBE-DMR data.

Novel methods have been recently developed based on other spaces where the data are transformed by either *filters*, *wavelets* or *eigenvectors*. Since the operations involved are linear the new coefficients should form a set of Gaussian variables if the underlying map is Gaussian. *Wavelets* are compensated filters which allow one to extract information which is localized in both real and harmonic space and for this reason they can be more sensitive than classical methods (for a detailed review of the properties of wavelets see [111]). In recent years they have been applied to the non-Gaussian analysis of the CMB. Many of the statistics and techniques used on real or harmonic space can be translated and applied to wavelet space (e.g., moments, scale-scale correlations, 1-point pdf). On small patches of the sky several *planar wavelet families* have been successfully applied to detect simulated cosmic strings embedded in a Gaussian signal [15] and search for discontinuities due to secondary anisotropies [4]. The *Haar wavelet* (the simplest wavelet that one can

construct) [228, 14] and the *Mexican Hat wavelet* (given by the Laplacian of a Gaussian) [153, 41] have been now implemented on the sphere (see Fig. 11 for an application of the latter wavelet to COBE). [153] has shown that the spherical Mexican Hat wavelet can be more sensitive than the spherical Haar wavelet for detecting types of non-Gaussianity expected in some non-standard scenarios. Moreover, the former wavelet has been found to be more sensitive than the bispectrum for constraining the nonlinear coupling parameter appearing in non-standard inflation using the COBE/DMR data [43]. Recently, *directional wavelets* having a preferred direction have been implemented on the sphere -e.g. *elliptical Mexican Hat* and *Morlet*- and applied to the CMB analyses [160]. The computational cost of exploring all possible directions can be greatly reduced by using *steerable wavelets* where the coefficients at any direction can be obtained as linear combinations of the ones of a basis with a limited number of elements [247, 248].

Filters can also help to extract non-Gaussian features from a given data set. This can be done in different ways, e.g. by removing the non-cosmological information (*Wiener*), equalizing the CMB signal (*signal-whitening*) or the noise (*noise-whitening*) [249] or taking *field derivatives* to study discontinuities (for an application to cosmic strings see [86]). In the noise-whitening case the corresponding signal-to-noise eigenvalues allow also a compression of the data (see [250]).

In addition to the CMB temperature, the determination of the statistical nature of polarization is crucial to test the Gaussianity of the CMB. Most of the tests proposed above for the temperature can be implemented for the CMB polarization. There are, however, other properties which are specific of the pseudo-vector nature of polarization. Up to now only a few tests have been developed based on *geometric characteristics of polarization*: peculiar points, up-crossing and down-crossing points of the modulus of polarization (see for instance [171]). In any case, it would be very desirable to devise methods combining temperature and polarization maps in an optimal way.

Some of the methods already discussed can as well be used to search for possible features present in the CMB maps arising from *global anisotropy*, *inhomogeneity* or *topology*. Particularly interesting are those based on wavelets, optimal filters and pattern recognition. If the universe is *anisotropic/inhomogeneous* (as in the case of, e.g., Bianchi, Tolman or Swiss-Cheese models) then the CMB temperature fluctuation field will be anisotropic/inhomogeneous on the sphere. The space-time geometry of the universe is expected to affect mainly the low-order multipoles (i.e. large angular scales). However, focusing of geodesics can also produce a large variety of features at smaller scales (e.g., hot spots, rings of fire, spiral patterns, North-South asymmetries, etc., see [19, 109]. For recent applications to detect those features in WMAP data see Sec. 6.2). If the *topology* of the universe is not trivial then anisotropic features will naturally appear in the CMB maps. Also symmetries are expected in some topologies (e.g. toroidal one). A method to probe non-trivial topology is based on the S-statistic which measures the symmetry of a map [223, 66]. An-

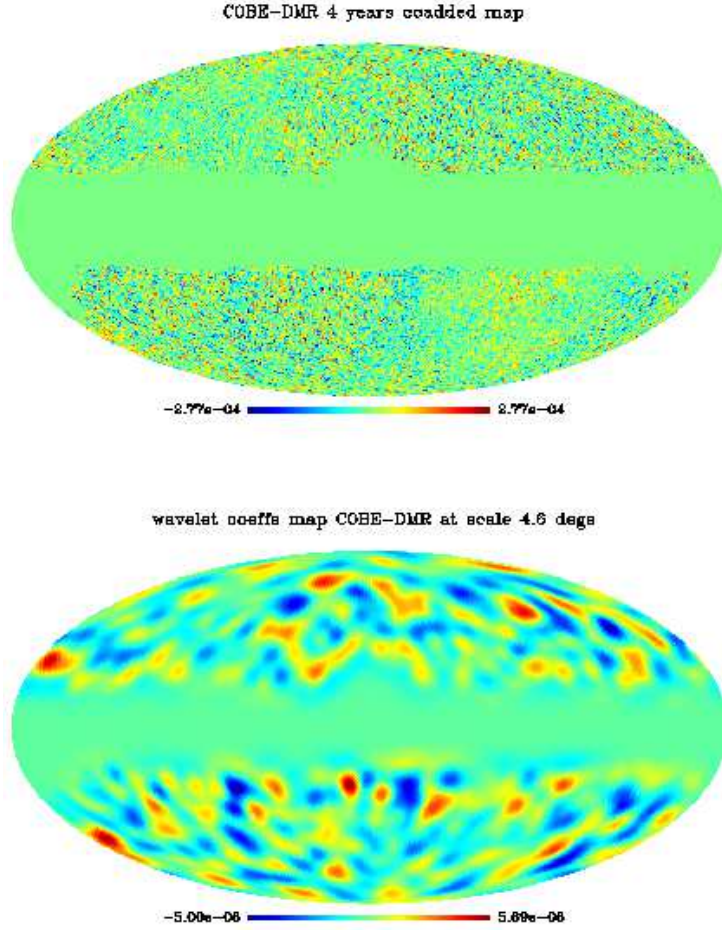


Fig. 11. Spherical Mexican Hat Wavelet coefficients for COBE-DMR (from [41]).

other technique consists on the *identified circles* principle. Circular patterns of temperature fluctuations are generated in compact topologies. A given circle should be seen in different positions of the CMB sky since it can travel to the observer following different geodesics. Notice, however, that it will not look exactly the same because of the ISW effect caused by different intervening structures and the Doppler effect at recombination whose projection on different geodesics will be also different. This technique has been applied to the COBE-DMR data [57, 58]. Techniques based on wavelets, that allow to detect the patterns of spots imprinted by the different topologies, have been implemented in [197]. The results show the potential of scale-scale correlations for distinguishing among different topologies. Recently, other techniques involv-

ing *phase correlations* have been applied to the WMAP data to constrain the topology of the universe [71].

6 Data analysis beyond the power spectrum

6.1 The Search for non-Gaussianity before WMAP

The first systematic analyses that have been done on CMB data in search for non-Gaussianity, have been performed on the 4 year COBE-DMR data set. This was for a decade the only whole-sky data set publicly available. The COBE-DMR data have been found to be compatible with the Gaussian hypothesis by the majority of the statistical tests applied. The few analyses finding deviations from normality have been later proved to be either incomplete or interpreted as undocumented systematic effects (see below). Monte Carlo simulations, taking into account all the instrumental and observational constraints of the data under analysis, are usually performed to estimate distributions of the testing-statistic as well as confidence levels.

The degree of asymmetry of the data was measured with the *3-point correlation function* (equilateral and pseudo-collapsed) by [120]. *Extrema distribution and correlations* of the temperature field have been tested by [120, 183]. Several works have relied on morphological characteristics of the observed field to detect non-Gaussianity, *the Minkowski functionals*, [207, 175] and in particular the *genus* (number of peaks above the threshold minus the number of holes. [120, 183]) to study the COBE-DMR data. The *Partition Function*, based on the combination of information at several scales and the contribution of different moments of the measure (defined in this case as the sum of absolute temperatures in a defined box), and the roughness of the last-scattering surface were proposed by [70] and [165], respectively, as powerful statistics to detect deviations from Gaussianity. All the analyses performed in those works were done in real space. No evidence of departure from Gaussianity of the COBE-DMR anisotropies was found in all the cases discussed above.

Tests were also carried out in spaces defined by eigenmodes and wavelets (see previous section). A *Principal Component Analysis* was done by [33] to extract the eigenmodes from the COBE-DMR data. χ^2 , Kolmogorov-Smirnoff, cumulants up to fourth order and significance of the top few outliers were calculated from the eigenmodes and tested against Gaussianity. None of these tests rejected the Gaussian hypothesis at the 95% confidence level. Skewness, kurtosis and scale-scale correlations of the COBE-DMR *Wavelet* coefficients have been studied in the north and south faces of the quad-cube COBE pixelization, using different wavelet bases [177, 169, 5]. Spherical wavelets have also been convolved with the COBE data (HEALPix pixelization) to test the distributions of wavelet coefficients at several scales against Monte Carlo simulations assuming Gaussianity [14, 41, 43]. A detection of non-Gaussianity was claimed by [177] finding the value of the scale-scale correlation (between

scales 11° and 22°) for the COBE data outside the 99% confidence level. However, [169] pointed out the orientation dependence of orthogonal wavelet basis. A rotation of the data by 180° makes the COBE data set compatible with Gaussianity.

Several works have studied the *bispectrum* of the COBE-DMR data in a simplified form that ignores correlations between different multipoles [77, 95, 12]. A rejection of Gaussianity was claimed by [77] at the 98% confidence level and appeared at $l = 16$. In a subsequent paper [12] analysed the bispectrum as a function of frequency, channel and time interval. The non-Gaussian signal was found to come only from the 53 GHz map, implying a non-cosmological origin. Removal of data corresponding to a period of time dominated by a systematic effect (data collected during an eclipse) resulted in a COBE-DMR bispectrum compatible with Gaussianity.

An *extended bispectrum* including components with correlations among different multipoles was studied by [147]. Gaussianity was rejected by the COBE-DMR data at a confidence level larger than 98%. An exhaustive study of the possible non-cosmological origin of this detection is included in that work giving negative results. With the aid of the WMAP data, this detection was later proved to be due to pixelization artifacts of the Quad-Cube tesselation of the sky and the eclipse data.

All the previous works calculated the COBE-DMR bispectrum for a limited number of modes. More recently, [124] have measured all the modes available from those data, 466 in total. They conclude that the data are consistent with Gaussianity. A recent study using the *trispectrum* also shows consistency with Gaussianity (having previously removed the data affected by the systematic effect, [126]).

While all the works mentioned above performed blind analyses, some works tried to detect deviations from Gaussianity in the form given by the *non-linear parameter* f_{NL} defined in Sec. 4.1. Only upper limits were obtained at least two orders of magnitude above the values expected in the most optimistic non-standard inflationary models (see e.g. [124, 43] for analyses involving the bispectrum and spherical wavelets, respectively).

Uncertainty remained about whether the CMB anisotropies are Gaussian distributed or not. Scales observed by the COBE-DMR experiment are above the causal horizon at the last-scattering surface. It could well be that even if the anisotropies are non-Gaussian distributed at smaller scales, they appear Gaussian above degree scales due to the central limit theorem. Therefore small angular scale observations are needed to answer this question. At present many of these new small scale observations have been tested against Gaussianity. The *genus* of the data of the balloon-borne QMAP, ground-based Saskatoon and QMASK (a combination of QMAP and Saskatoon) experiments was compared to Gaussian predictions by [178]. Only in the case of QMASK was an asymmetry in the genus curve found. However this deviation from the Gaussian genus curve was not statistically significant. [209] calculated several *morphological quantities* from the QMASK data and con-

cluded that they were consistent with the values expected for a Gaussian field. Several statistics have been computed to test the Gaussianity of the balloon-borne MAXIMA-1 data [250, 203, 42, 6]. [250] apply *moments*, *cumulants*, *the Kolmogorov-Smirnov test*, *the χ^2 test*, and *Minkowski functionals* in eigen, real, Wiener-filtered and signal-whitened spaces; [203] estimate the *bispectrum*; [42, 6] apply *goodness-of-fit* tests to the data. Consistency with Gaussianity was found in all cases. The balloon observations of BOOMERanG maps were also searched for deviations from Gaussianity. [188] perform a real-space analysis, computing *skewness*, *kurtosis* and *Minkowski functionals* of those data. No significant deviation from Gaussianity was found.

More recently and contemporary to the WMAP analyses, the statistical distribution of interferometric observations taken with the VSA experiment have been also examined. [205] apply some tests in real and harmonic spaces, the former to the maximum-entropy reconstruction of the observed regions. [218] focus on the *bispectrum* of the data. [201] apply *smooth tests of goodness-of-fit* developed by [7]. The results of the analyses seem to be in relatively good agreement with the Gaussian assumption (except for maybe one or two fields in the analysis of [201]).

6.2 WMAP and non-Gaussianity

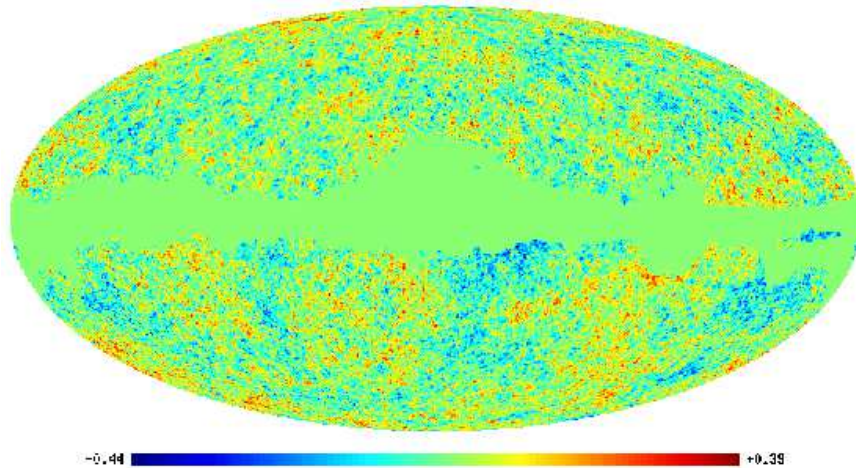


Fig. 12. The first year WMAP combined, foreground cleaned Q-V-W map together with the kp0 mask.

The quality of the first-year all-sky data provided by the WMAP satellite has motivated many works dealing with the Gaussianity and isotropy of the CMB signal (also in relation to the geometry and topology of the universe,

see Sec. 4.2). Clean maps are constructed by the WMAP team and made publicly available to the community, together with noise templates and beam responses for all the channels. Also a mask is provided to ignore those pixels in the analysis where the foreground contamination is believed to be unavoidable. All this information is essential to perform “realistic” simulations of the data needed to compare the values of the chosen statistics with the ones obtained from the true data. Fig. 12 shows the first-year WMAP map obtained after a noise-weighted combination of the foreground cleaned Q-V-W channels (hereafter WCM). Although other foreground cleaned maps have been produced based on different techniques [22, 225, 76, 180], for non-Gaussianity studies the WCM (together with the most conservative kp0 mask) is preferred since the noise properties are well defined for this map.

There have been a wide range of analyses of the temperature distribution using different quantities. *Minkowski functionals* have been computed by [125, 51, 179, 148, 74]. The results obtained from those works are diverse: whereas compatibility with Gaussianity is found in [125, 51], others find significant deviations from it [179, 148, 74]. The main reason for the discrepancy is that, although based on the same quantities, they construct different measures from them as the asymmetry in the genus above/below a given threshold or in different hemispheres (these latter asymmetries have also been found in the power spectrum or the n -point correlation functions for different regions of the sky, see below).

N-point correlation functions have been calculated by [83, 75] for the temperature. [75] find North-South asymmetries on large scales in ecliptic coordinates. Statistics based on the *alignment of low-multipoles* have been computed by [66, 56, 222, 217, 245, 130, 25]. Uncomfortably low probability for the observed quadrupole and octopole alignment has been obtained in those works (the so-called axis of evil). The *bispectrum* have been calculated for different subsets of all its components up to the WMAP resolution [125, 132, 39]. Significant non-null results have been obtained in several of those analyses which agree well with the emission expected from undetected point sources [125, 10]. In addition those results can be translated to limits on the non-linear parameter f_{NL} [125, 39]. By using another subset of multipole configurations, namely the closest inter- ℓ components, [132] have also found North-South asymmetries in agreement with previous results [75, 92].

Phase correlations have been used to test the hypothesis that the CMB temperature fluctuations on the celestial sphere constitute a homogeneous and isotropic Gaussian random field. This hypothesis implies that the phases of the spherical harmonic coefficients corresponding to the temperature fluctuations are independent and uniformly distributed in the interval $[0, 2\pi]$. Phase analyses of different derived maps of the WMAP data have been performed by [49, 172, 50, 173]. These works find departures from uniformity and/or independency which in general reflect galactic contamination or noise gradients rather than primordial non-Gaussianity.

Several statistics based on the *spherical wavelet coefficients* of the CMB data have been used to test the Gaussian hypothesis [238, 170, 160, 62, 44, 143]. Highly significant deviations have been found in the *kurtosis* of the WMAP data for both *symmetric* [238, 170] and *directional wavelets* [160]. An analysis of *extrema of the wavelet coefficients* identifies a very *cold spot* as the cause of the large kurtosis found with the *spherical Mexican Hat wavelet* [62] (see Fig. 13). This cold spot has been also revealed by the *higher criticism* test applied to the wavelet coefficients [44]. Moreover, [63] find a nearly spherical shape for the cold spot and also that it cannot be explained with foreground emissions. A test of global isotropy has been recently performed by [248] using *steerable wavelets*. Convolving the CMB map with the steerable wavelet given by the second derivative of the Gaussian at a fixed scale, a preferred orientation is signaled by the maximum of the coefficients corresponding to the different orientations and assigned to each pixel. Each pixel is thus looking at all the pixels intersected by the great circle formed by extrapolating the preferred orientation. Then the number of times each pixel is seen by any other pixel is counted. In the case of a homogeneous and isotropic Gaussian random field all the pixels are seen the same number of times on average. Performing this test on the WMAP first-year data, a number of anomalous directions were found at a very high significance level. Their mean direction is very close to the ecliptic poles, being $\approx 10^\circ$ from it (see Fig. 14). Moreover, the anomalous directions are located along a great circle whose perpendicular is pointing towards a direction close to the dipole and to the axis of evil. This result synthesise for the first time the previously reported anomalies commented above on the North-South asymmetry and the alignment of low-multipoles. Contrary to these results, analyses based on the bipolar spectra do not find violation of the global isotropy of the universe [89, 90].

Number and correlation of extrema are computed by [134, 135, 232]. [134, 135] find that the maxima and minima in the WMAP data are not hot and cold enough. [232] find evidence for non-Gaussianity on large scales which could be associated with residual foregrounds.

Local curvature has been investigated by [93, 38]. They classify the points in the data as hills, lakes or saddles according to the sign of the eigenvalues of the Hessian matrix, and consider the proportions of each of them above a certain threshold. A clear asymmetry is found which is maximum for hemispheres centered near the ecliptic poles, consistent with the results by [75].

Several suggestions have been made to explain the anomalies found in the first-year WMAP data at the large angular scales, namely the power deficit and alignment of the low-order multipoles, the asymmetries between different hemispheres and the cold spot⁴.

A suggestion to explain the low-multipole anomaly invokes a non-trivial topology which due to the finite size of the universe tends to cut power at the lowest multipoles and in some cases to align them [144, 199, 11]. However,

⁴These anomalies remained almost unaltered in the 3-years WMAP data.

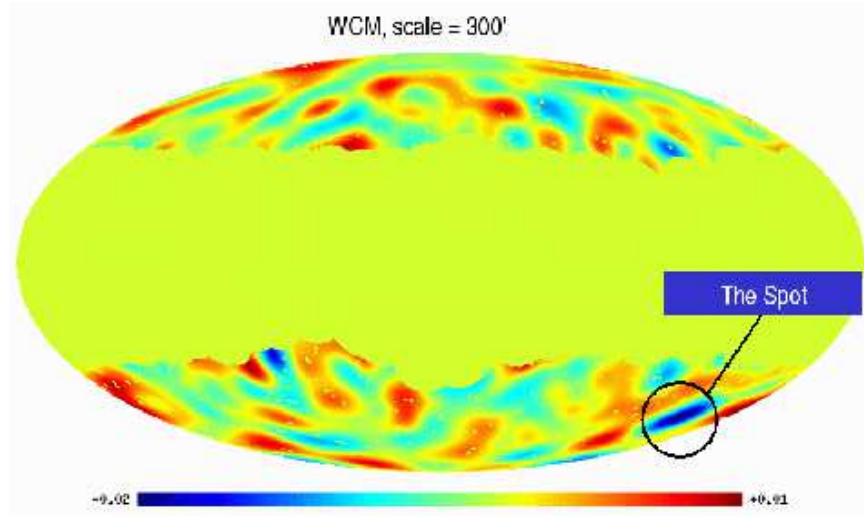


Fig. 13. The Cold Spot found in the WMAP combined map after convolving with a Spherical Mexican Hat Wavelet with scale 300' (see [238, 62, 63])

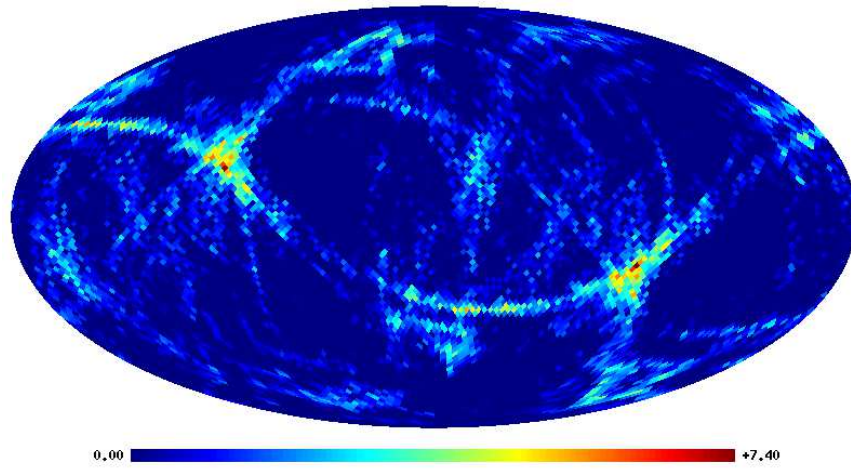


Fig. 14. Excess of the number of times each pixel is seen by any other in σ units, where σ is the dispersion corresponding to Gaussian simulations (see [248])

apart from this nice consequence, there is no evidence for a possible non-trivial topology. Another possibility proposed is the lensing of the dipole by local large-scale structures which can potentially produce a quadrupole and octopole similar to those found in the WMAP data [236]. It remains to be demonstrated that the appropriate physical characteristics of those structures (in terms of mass, size and position) are in fact present in the local universe.

Possible explanations for the cold spot are the RS effect produced by the most prominent voids or massive structures in the universe [151, 233, 107], topological defects in the form of textures [234] or, a more radical one, based on an inhomogeneous model of the universe given by a finite sphere of dust and dark energy [2].

Anisotropic and inhomogeneous geometries leaving spiral or stripy patterns in the CMB sky have been proposed to correct the large-angle anomalies found (asymmetries, the cold spot and the low-multipole power deficit and alignment) [108, 131, 45, 32] (see however [162] for further non-Gaussian detections in the Bianchi VII_h corrected WMAP first year data). Although a good fit can be found for most of the anomalies with the anisotropic geometries (Bianchi VII_h) however the values required for the matter content are too high [109, 32].

Small changes in the magnitude of the WMAP dipole vector [80], together with possible systematics or foreground residuals associated with the ecliptic (as might be inferred from the recent results by [75, 92, 248]), might be considered as a possibility to explain the large-scale anomalies. However much more work is still needed in order to find a convincing case for them.

7 Conclusions

Cosmology is passing through a period of abundance of new data which imply a significant improvement on the precision in the determination of the parameters characterizing the universe. The CMB field is probably the major contributor to that improvement and is expected to be so in the next decade. With only the first year of WMAP data, the power spectrum of the temperature anisotropies has been determined with error bars below cosmic variance up to multipoles $\ell \approx 600$. Information on larger multipoles is already provided by several high-resolution experiments allowing a consistent determination of the third acoustic oscillation and providing an incomplete coverage of the multipoles up to $\ell \approx 2500$. In the next few years, the ESA Planck mission is expected to provide accurate and high resolution all-sky images of the CMB temperature anisotropies in a wide frequency range which will allow an optimal removal of foregrounds and a very good control of systematics. From those high quality images a complete coverage of multipoles at the cosmic variance limit will be obtained up to $\ell \approx 2500$. The C_ℓ so obtained will be the ultimate temperature power spectrum of the primary CMB anisotropies since

secondary anisotropies are expected to start to be dominant beyond those multipoles.

The large-scale galaxy surveys as well as the high- z SN Ia light curves have also played a crucial role in establishing the concordance model. The strong complementarity of these two cosmological data sets with the CMB anisotropies has implied a significant improvement on the parameter determination compared to each data set considered individually. And, what is more important, a consistency check of the best fit model. In the next years, that combination of data sets is expected to be strengthened with weak lensing observations of background galaxies in large areas of the sky.

In addition to the power spectrum, the recent studies on the statistical distribution of the temperature anisotropies provide independent tests of the standard inflationary model. Significant deviations from a homogeneous and isotropic Gaussian random field have already been found in the first-year WMAP data. However the origin of those deviations, whether cosmological, residual foregrounds or systematics, is still a matter of debate. More precised maps from next years of WMAP data and specially the high quality maps expected from the Planck mission will certainly help in the clarification of the possible causes of the anomalies found.

Finally, high sensitive polarization maps to search for the B-mode will be the next major quest after Planck. The B-mode polarization is at present the best way to study the primordial background of gravitational waves expected in the standard model of inflation. It is therefore not surprising that both space agencies, NASA and ESA, have considered polarization missions in their future programs “Beyond Einstein” and “Cosmic Vision”, respectively.

Acknowledgments

I thank J.L. Sanz and P. Vielva for useful comments on the manuscript. I acknowledge financial support from the Spanish MEC project ESP2004-07067-C03-01. I also acknowledge the use of LAMBDA, support for which is provided by the NASA Office of Space Science. I acknowledge the use of the software package CMBFAST (<http://www.cmbfast.org>) developed by Seljak and Zaldarriaga. The work has also used the software package HEALPix (<http://www.eso.org/science/healpix>) developed by K.M. Gorski, E.F. Hivon, B.D. Wandelt, J. Banday, F.K. Hansen and M. Barthelmann.

References

1. Abazajian K. et al., 2004, *AJ*, 128, 502
2. Adler R.J., Bjorken J.D. & Overduin J.M., 2006, [gr-qc/0602102](http://arxiv.org/abs/gr-qc/0602102)
3. Aghanim N., Desert F.X., Puget J.L. & Gispert R., 1996, *A&A*, 311, 1.
4. Aghanim N., Forni O. 1999, *A&A*, 347, 409
5. Aghanim N., Forni O. & Bouchet F.R., 2001, *A&A*, 365, 341-346

6. Aliaga A.M., Martínez-González E., Cayón L., Argüeso F., Sanz J.L. & Barreiro R.B., 2003, *New Astron. Rev.*, 47, 821
7. Aliaga A.M., Rubiño-Martín J.A., Martínez-González E., Barreiro R.B. & Sanz J.L., 2005, *MNRAS*, 356, 1559
8. Afshordi N., Loh Y.-S. & Strauss M. A., 2004, *Phys. Rev. D*, 69, 3524
9. Allen A.W., Schmidt R.W. & Fabian A.C., 2002, *MNRAS*, 334, L11
10. Argüeso F., González-Nuevo J. & Toffolatti L., 2003, *ApJ*, 598, 86-96
11. Aurich R., Lustig S. & Steiner F., 2006, *MNRAS*, 369, 240, astro-ph/0510847
12. Banday A.J., Zaroubi S. & Gorski K.M., 2000, *ApJ*, 533, 575-587
13. Barreiro R.B., Sanz J.L., Martínez-González E. & Silk J., 1998, *MNRAS*, 296, 693
14. Barreiro R.B., Hobson M.P., Lasenby A.N., Banday A.J., Gorski K.M. & Hinshaw G., 2000, *MNRAS*, 318, 475-481
15. Barreiro R.B. & Hobson M.P., 2001, *MNRAS*, 327, 813, astro-ph/0104300
16. Barreiro R.B., Martínez-González E. & Sanz J.L. 2001, *MNRAS*, 322, 411
17. Barreiro R.B., 2006, in this volume, astro-ph/0512538
18. Barreiro R.B., Martínez-González E., Vielva P. & Hobson M.P., 2006, *MNRAS*, 368, 226
19. Barrow J.D., Juszkiewicz R. & Sonoda D.H., 1985, *MNRAS*, 213, 917
20. Bartelmann M. & Schneider P., 2001, *Phys. Rep.* 340, 291
21. Bartolo N., Komatsu E., Matarrese S. & Riotto A., 2004, *Phys. Rep.*, 402, 103
22. Bennett C.L. et al., 2003, *ApJS*, 148, 1
23. Bersanelli M., Maino, D. & Mennella A., 2002, *Nuovo Cimento*, 25, 1
24. Bevis N., Hindmarsh M. & Kunz M., 2004, *Phys. Rev. D*, 70, 043508
25. Bielewicz P., Eriksen H.K., Banday A.J., Górski K.M. & Lilje P.B., 2005, *ApJ*, 635, 750
26. Boldt E., 1987, *Phys. Rev.*, 146, 215
27. Bond J.R. & Efstathiou G., 1987, *MNRAS*, 226, 655
28. Bond J.R. et al., 2005, *ApJ*, 626, 12
29. Bouchet F.R. & Gispert R., 1999, *New Astronomy Reviews*, 4, 443
30. Bouchet F.R., Benoît A., Camus Ph., Désert F.X., Piat M. & Ponthieu N., 2005: Charting the New Frontier of the Cosmic Microwave Background Polarization. In: *SF2A*, ed. by F. Casoli et al. (EDP Sciences 2004), astro-ph/0510423
31. Boughn S.P. & Crittenden R.G., 2004, *Nature*, 427, 45
32. Bridges M., Lasenby A.N. & Hobson M.P., 2006, *MNRAS Letters*, submitted, astro-ph/0605325
33. Bromley B.C. & Tegmark M., 1999, *ApJ*, 524, L79-L82.
34. Bucher M., Moodley K. & Turok N., 2001, *Phys. Rev. Lett.*, 87, 191301
35. Bunn, E.F., Ferreira, P. & Silk, J. 1996, *Phys. Rev. Lett.*, 77, 2883
36. Bunn E.F., Zaldarriaga M., Tegmark M. & de Oliveira-Costa A., 2003, *Phys. Rev. D*, 67, 023501
37. Cabella, P. & Kamionkowski, M., 2004, Theory of Cosmic Microwave Background Polarization. In: *The Polarization on the Cosmic Microwave Background*, 2003 Villa Mondragone School of Gravitation and Cosmology, Rome, September 6-11, astro-ph/0403392
38. Cabella P., Liguori M., Hansen F.K., Marinucci D., Matarrese S., Moscardini L. & Vittorio N., 2005, *MNRAS*, 358, 684
39. Cabella P., Hansen F.K., Liguori M., Marinucci D., Matarrese S., Moscardini L. & Vittorio N., 2006, *MNRAS*, 369, 819, astro-ph/0512112

40. Castro P.G., 2003, Phys. Rev. D, 67, 123001, astro-ph/0212500
41. Cayón L., Sanz J.L., Martínez-González E., Banday A.J., Argüeso F., Gallegos J.E., Gorski K.M. & Hinshaw G., 2001, MNRAS, 326, 1243
42. Cayón L., Argüeso F., Martínez-González E. & Sanz, 2003, MNRAS, 344, 917
43. Cayón L., Martínez-González E., Argüeso F., Banday A.J., Gorski K.M., 2003, MNRAS, 339, 1189
44. Cayón L., Jin L. & Treaster A., 2005, MNRAS, 362, 826
45. Cayón L., Banday A.J., Jaffe T., Eriksen H.K., Hansen F.K., Gorski K.M. & Jin J., 2006, MNRAS, 369, 598
46. Challinor A., 2004, Anisotropies in the Cosmic Microwave Background. In: *Proceedings of the 2nd Aegean Summer School on the Early Universe*, 22-30 September 2003, to appear in Springer LNP, astro-ph/0403344
47. Challinor A., 2006, in this volume, astro-ph/0502093
48. Challinor A. & Chon G., 2005, MNRAS, 360, 509
49. Chiang L.-Y., Naselsky P.D., Verkhodanov O.V. & Way M.J., 2003, ApJL, 590, 65
50. Coles P., Dineen P., Earl J. & Wright D., 2004, MNRAS, 350, 989
51. Colley W.N. & Gott J.R., 2003, MNRAS, 344, 686
52. Condon J.J. et al., 1998, AJ, 115, 1693
53. Contaldi C.R., Ferreira P.G. & Magueijo J., 2000, ApJ, 534, 25
54. Cooray, A.R. & Hu, W. 2000, ApJ, 534, 533
55. Cooray, A. 2001, Phys. Rev., D64, 063514, astro-ph/0105063
56. Copi C.J., Huterer D. & Starkman G.D., 2004, Phys. Rev. D, 70, 043515, astro-ph/0310511
57. Cornish N.J., Spergel D.N. & Starkman G.D., 1996, Phys. Rev. Lett., 77, 215
58. Cornish N.J., Spergel D.N. & Starkman G.D., 1998, Class. Quant. Grav., 15, 2657-2670
59. Cresswell J.G., Liddle A.R., Mukherjee P. & Riazuelo A., 2006, Phys. Rev. D, 73, 041302, astro-ph/0512017
60. Croft R.A.C. et al., 2002, ApJ, 581, 20
61. Crotty P., Lesbourgues J. & Pastor S., 2003, Phys. Rev. D, 67, 123005
62. Cruz M., Martínez-González E., Vielva P. & Cayón L., 2005, MNRAS, 356, 29
63. Cruz M., Tucci M., Martínez-González E. & Vielva P., 2006, MNRAS, 369, 57
64. de Bernardis P. et al., 2000, Nature, 404, 955
65. de Oliveira-Costa A., Smoot G.F. & Starobinsky A.A., 1996, ApJ, 468, 457
66. de Oliveira-Costa A., Tegmark M., Zaldarriaga M. & Hamilton A., 2004, Phys. Rev. D, 69, 063516
67. Delabrouille R.B., 2006, in this volume.
68. Delabrouille J., Cardoso J.-F. & Patanchon G., 2003, MNRAS, 346, 1089
69. Dickinson C. et al., 2004, MNRAS, 353, 732
70. Diego J.M., Martínez-González E., Sanz J.L., Mollerach S. & Martínez V.J., 1999, MNRAS, 306, 427-436
71. Dineen P., Rocha G. & Coles P., 2005, MNRAS, 358, 1285
72. Doré O., Colombi S. & Bouchet F.R., 2003, MNRAS, 344, 905
73. Efstathiou G., 2004, MNRAS, 348, 885
74. Eriksen H.K., Novikov D.I., Lilje P.B., Banday A.J., Gorski K.M., 2004, ApJ, 612, 64
75. Eriksen H.K., Hansen F.K., Banday A.J., Gorski K.M. & Lilje P.B., 2004, ApJ, 605, 14

76. Eriksen H.K., Banday A.J., Gorski K.M. & Lilje P.B., 2004, *ApJ*, 612, 633
77. Ferreira P.G., Magueijo J. & Gorski K.M., 1998, *ApJ*, 503, L1-L4
78. Fosalba P., Gaztañaga E. & Castander F., 2004, *ApJL*, 597, 89
79. Fraisse A.A., 2005, *Phys. Rev. Lett.*, submitted, astro-ph/0503402
80. Freeman, P.E., Genovese, C.R., Miller, C.J., Nichol, R.C. & Wasserman, L., 2006, *ApJ*, 638, 1
81. Freedman W.L. et al., 2001, *ApJ*, 553, 47
82. Gaztañaga E., Fosalba P. & Elizalde E., 1998, *MNRAS*, 295, L35-L39
83. Gaztañaga E. & Wagg J., 2003, *Phys. Rev. D*, 68, 021302
84. Goldberg D.M. & Spergel D.N., 1999, *Phys. Rev. D* 59, 103002.
85. Gorski K.M., Hivon E., Banday A.J., Wandelt B.D., Hansen F.K., Reinecke M. & Bartelman M. 2005, *ApJ*, 622, 759
86. Gott J. R. III, Park, C., Juskiewicz, R., Bies, William E., Bennett, D. P., Bouchet, F.R., Stebbins, A. 1990, *ApJ*, 352, 1
87. Graham P., Turok N. Lubin P.M. & Schuster J.A., 1995, *ApJ*, 449, 404-412
88. Gruzinov, A. & Hu, W. 1998, *ApJ*, 508, 435.
89. Hajian A. & Souradeep T., 2003, *ApJ*, 597, 5
90. Hajian A., Souradeep T. & Cornish N., 2005, *ApJ*, 618, 63
91. Hanany S. et al., 2000, *ApJ*, 545, L5
92. Hansen F.K., Banday A.J. & Gorski K.M., 2004, *MNRAS*, 354, 641
93. Hansen F.K., Cabella P., Marinucci D. & Vittorio N., 2004, *ApJ*, 607, L67
94. Hawkins E. et al., 2003, *MNRAS*, 346, 78
95. Heavens A.F., 1998, *MNRAS*, 299, 805-808.
96. Heavens A.F. & Sheth R.K., 1999, *MNRAS*, 310, 1062
97. Heavens A.F. & Gupta S., 2000, *MNRAS*, 324, 960, astro-ph/0010126
98. Herranz D., Sanz J.L., Hobson M.P., Barreiro R.B., Diego J.M., Martínez-González E. & Lasenby A.N., 2002, *MNRAS*, 336, 1057
99. Hinshaw G. et al., 2003, *ApJ*, 148, 135
100. Hipólito-Ricaldi W.S. & Gomero G.I., 2005, *Phys. Rev. D*, 72, 103008
101. Hobson M.P., Jones A.W., Lasenby A.N. & Bouchet F., 1998, *MNRAS*, 300
102. Hu W., 2000, *Phys. Rev. D*, 62, 043007
103. Hu W., 2001, *Phys. Rev. D*, 64, 083005
104. Hu W. and Dodelson S., 2002, *ARAA*, 40, 171
105. Hu W. & Okamoto T., 2002, *ApJ*, 574, 566
106. Inoue K.T., 2001, *Prog. Theor. Phys.*, 106, 39, astro-ph/0102222
107. Inoue K.T. & Silk J., 2006, *ApJ*, 648, 23
108. Jaffe T.R., Banday A.J., Eriksen H.K., Gorski K.M. & Hansen F.K., 2005, *ApJL*, 629, L1, astro-ph/0503213
109. Jaffe T.R., Hervik S., Banday A.J., Gorski K.M., 2006, *ApJ*, 644, 701, astro-ph/0512433
110. Jassal H.K., Bagla J.S. & Padmanabhan T., 2005, astro-ph/0506748
111. Jones B.J.T., 2006, in this volume
112. Jones W.C. et al., 2006, *ApJ*, 647, 823, astro-ph/0507494
113. Kamionkowski M., Kosowsky A. & Stebbins A., 1997, *Phys. Rev. D*, 55, 7368
114. Kendall M.G. & Stuart A., 1977, *The Advance Theory of Statistics*, London: Charles Griffin
115. Kesden M., Cooray A. & Kamionkowski M., 2003, *Phys. Rev. D*, 67, 123507
116. Kinney W.H., 2002, *Phys. Rev. D*, 66, 083508
117. Knop R.A. et al., 2003, *ApJ*, 598, 102

118. Knox, L., Scoccimarro, R. & Dodelson, S. 1998, Phys. Rev. Lett., 81, 2004
119. Knox L. & Song Y.-S., 2002, Phys. Rev. Lett., 89, 011303
120. Kogut A., Banday A.J., Bennett C.L., Gorski K.M., Smoot G.F. & Wright E.L., 1996, ApJ, 464, L29-L33.
121. Kogut A., Hinshaw G. & Banday A.J., 1997, Phys. Rev. D, 55, 1901
122. Kogut A. et al., 2003, ApJS, 148, 161
123. Kovac J.M. et al. 2002, Nature, 420, 772
124. Komatsu E., Wandelt B.D., Spergel D.N., Banday A.J. & Gorski K.M., 2002, ApJ., 566, 19
125. Komatsu E. et al., 2003, ApJS, 148, 119
126. Kunz M., Banday A.J., Castro P.G., Ferreira P.G. & Gorski K.M., 2001, ApJ, 563, 99
127. Kunz M., Aghanim N., Cayón L., Forni O. & Riazuelo A., 2006, Phys. Rev. D, 73, 023511, astro-ph/0510164
128. Kuo C.L. et al., 2004, ApJ, 600, 32
129. Lachièze-Rey, M. & Luminet, J.-P. 1995, Phys. Rep., 254, 135
130. Land K. & Magueijo J., 2005, Phys. Rev. Lett., 95, 071301
131. Land K. & Magueijo J., 2005, MNRAS, 367, 1714, astro-ph/0509752
132. Land K. & Magueijo J., 2005, MNRAS, 357, 994
133. Landriau M. & Shellard E.P.S., 2004, Phys. Rev. D, 69, 023003
134. Larson D.L. & Wandelt B.D., 2004, ApJ, 613, 85
135. Larson D.L. & Wandelt B.D., 2005, Phys. Rev. D, submitted, astro-ph/0505046
136. Leitch E.M., Kovac J.M., Halverson N.W., Carlstrom J.E., Pryke C. & Smith M.W.E., 2005, ApJ, 624, 10, astro-ph/0409357
137. Levin J., 2002, Phys. Rep., 365, 251-333
138. Lewis A., Challinor A. & Lasenby A., 2000, ApJ, 538, 473, <http://camb.info>
139. Lewis A., Challinor A. & Turok N., 2002, Phys. Rev. D, 65, 023505
140. Lewis A., 2004, Phys. Rev. D, 70, 043011
141. Liddle A.R. & Lyth D.H., 2000, *Cosmological Inflation and Large-Scale Structure*, Cambridge University Press
142. Liguori M., Hansen F.K., Komatsu E., Matarresse S. & Riotto A., 2006, Phys. Rev. D, 73, 043505
143. Liu X. & Zhang S.N., 2005, ApJ, 633, 542
144. Luminet J.-P., Weeks J.R., Riazuelo A., Lehoucq R. & Uzan J.-P., 2003, Nature, 425, 593
145. Lyth D.H. & Wands D., 2002, Phys. Lett. B, 524, 5
146. Maffei B. et al., 2005, EAS Publications Series, 14, 251-256
147. Magueijo J., 2000, ApJ, 528, L57-L60
148. Magueijo J. & Medeiros J., 2004, MNRAS, 351, L1
149. Maino D. et al., 2002, MNRAS, 334, 53
150. Martínez-González E., Sanz J.L. & Silk J., 1990, ApJL, 335, L5
151. Martínez-González E. & Sanz J.L., 1990, MNRAS, 247, 473
152. Martínez-González, E. & Sanz, J.L. 1995, A&A, 300, 346
153. Martínez-González E., Gallegos J.E., Argüeso F., Cayón L., Sanz J.L., 2002, MNRAS, 336, 22
154. Martínez-González E., Diego J.M., Vielva P. & Silk J., 2003, MNRAS, 345, 1101
155. Martínez-González E. & Vielva P., 2005: The Cosmic Microwave Background Anisotropies: Open Problems. In: *JENAM Workshop: The Many Scales in the Universe*, ed. by C. del Toro et al., (Kluwer), astro-ph/0510003

156. Masi S. et al., 2005, EAS Publications Series, 14, 87-92
157. Mather J.C. et al. 1994, ApJ, 420, 439
158. Mather J.C. et al. 1999, ApJ, 512, 511
159. McDonald P. et al., 2005, ApJ, 635, 761, astro-ph/0407377
160. McEwen J. D., Hobson M. P., Lasenby A. N. & Mortlock D. J., 2005, MNRAS, 359, 1583
161. McEwen J.D., Vielva P., Hobson M.P., Martínez-González E. & Lasenby A.N., 2006, MNRAS, submitted, astro-ph/0602398
162. McEwen J. D., Hobson M. P., Lasenby A. N. & Mortlock D. J., 2005, MNRAS, 359, 1583
163. Mennella A. et al., 2004, Recent Research Developments in Astronomy and Astrophysics, submitted, astro-ph/0402528
164. Mollerach S., Gangui A., Luchin F., Matarrese S., 1995, ApJ, 453, 1
165. Mollerach S., Martínez V. J., Diego J. M., Martínez-González E., Sanz J. L., Paredes S., 1999, ApJ, 525, 17
166. Monteserín C., Barreiro R.B., Sanz, J.L. & Martínez-González E., 2005, MNRAS, 360, 9
167. Monteserín C., Barreiro R.B., Martínez-González E. & Sanz J.L., 2006, MNRAS, 371, 312
168. Montroy T.E. et al., 2006, ApJ, 647, 813, astro-ph/0507514
169. Mukherjee P., Hobson M.P. & Lasenby A.N., 2000, MNRAS, 318, 1157-1163
170. Mukherjee P. & Wang Y., 2004, ApJ, 613, 51
171. Naselsky P.D. & Novikov D.I., 1998, ApJ, 507, 31
172. Naselsky P.D., Doroshkevich A.G. & Verkhodanov O.V., 2003, ApJL, 599, L53
173. Naselsky P., Chiang L.-Y., Olesen P. & Novikov I., 2005, Phys. Rev. D, 72, 063512
174. Nolta M. R. et al., 2004, ApJ, 608, 10
175. Novikov D., Schmalzing J. & Mukhanov V.F., 2000, A& A, 364, 17-25
176. Ostriker J.P. & Vishniac E.T., 1986, ApJ, 306, 510
177. Pando J., Valls-Gabaud D. & Fang L.-Z., 1998, Physical Review Letters, 81, 4568-4571
178. Park C.-G., Park C., Ratra B. & Tegmark M., 2001, ApJ, 556, 852, astro-ph/0102406
179. Park C.-G., 2004, MNRAS, 349, 313
180. Patanchon G., Cardoso J.-F., Delabrouille J. & Vielva P., 2005, MNRAS, 364, 1185
181. Percival W.J. et al., 2001, MNRAS, 327, 1297
182. Perlmutter S., 1999, ApJ, 517, 565
183. Phillips N.G. & Kogut A., 2001, ApJ, 548, 540-549.
184. Piacentini F. et al., 2005, ApJ, 647, 823, astro-ph/0507507
185. The Planck Consortia, 2005, in Planck: The Scientific Programme, European Space Agency, ESA-SCI(2005)1
186. Pogossian, L., Tye, S.-H.H., Wasserman, I. & Wyman, M., 2003, Phys. Rev. D, 68, 0235506
187. POLARBEAR, <http://bolo.berkeley.edu/polarbear>
188. Polenta G. et al., 2002, ApJ, 572, L27, astro-ph/0201133
189. QUIET, <http://quiet.uchicago.edu>
190. Rapetti D., Steven S.W. & Weller J., 2005, MNRAS, 360, 555
191. Readhead A.C.S. et al., 2004, ApJ, 609, 498

192. Readhead A.C.S. et al., 2004, *Science*, 306, 836
193. Riazuelo, A., Uzan, J.-P., Lehoucq, R. & Weeks, J., 2004, *Phys. Rev. D*, 69, 103514, astro-ph/0212223
194. Riess et al., 1998, *ApJ*, 116, 1009
195. Riess et al., 2001, *ApJ*, 560, 49
196. Rocha G., Magueijo J., Hobson M. & Lasenby A., 2001, *Phys. Rev. D*, 64, 063512, astro-ph/0008070
197. Rocha G., Cayón L., Bowen R., Canavezes A., Silk J., Banday A.J. & Gorski K.M., 2004, *MNRAS*, 351, 769, astro-ph/0205155
198. Roukema, B., 2000, *MNRAS*, 312, 712
199. Roukema B.F., Lew B., Cechowska M., Marecki A. & Bajtlik S., 2004, astro-ph/0402608
200. Rees M.J. & Sciama D.W., 1968, *Nature*, 517, 611
201. Rubiño-Martín et al., 2006, *MNRAS*, 369, 909
202. Sachs R. K. & Wolfe A. M., 1967, *ApJ*, 147, 73
203. Santos M.G. et al., 2002, *Phys. Rev. Lett.*, 88, 241302, astro-ph/0107588
204. Sanz J.L., 1997, in *The Cosmic Microwave Background*, eds. C.H. Lineweaver et al., Kluwer Academic Publishers, p. 33
205. Savage R. et al., 2004, *MNRAS*, 349, 973
206. Scannapieco, E., Levin and Silk, J. 1999, *MNRAS*, 303, 797
207. Schmalzing J. & Gorski K.M., 1998, *MNRAS*, 297, 355.
208. Scott D.H., Srednicki M. & White M., 1994, *ApJ*, 421, 5
209. Shandarin S.F., Feldman H.A., Xu Y. & Tegmark M., 2002, *ApJS*, 141,1, astro-ph/0107136
210. Seljak U. et al., 2005, *Phys. Rev. D*, 71, 103515
211. Seljak U. & Hirata C.M., 2004, *Phys. Rev. D*, 69, 043005
212. Seljak U., Sugiyama N., White M. & Zaldarriaga M., 2003, *Phys. Rev. D*, 68, 3507
213. Seljak U. & Zaldarriaga M., 1996, *ApJ*, 469, 437 (<http://www.cmbfast.org>)
214. Seljak U. & Zaldarriaga M., 1999, *Phys. Rev. D*, 60, 043504.
215. Silk J., 1968, *ApJ*, 151, 459
216. Skrutskie M.F. et al., 1997, in *The Impact of Large Scale Near-IR Sky Survey*, eds. Gazón F. et al., Kluwer, Dordrecht, p. 187
217. Slosar A. & Seljak U., 2004, *Phys. Rev. D*, 70, 083002
218. Smith S. et al., 2004, *MNRAS*, 352, 887
219. Smoot G. F. et al., 1992, *ApJL*, 396, L1
220. Spergel D. N. et al., 2003, *ApJS*, 148, 175
221. Sunyaev R.A. & Zeldovich Y.B., 1972, *Comm. Astrophys. Space Phys.*, 4, 173
222. Schwartz D.J., Starkman, G.D., Huterer D. & Copi C.J., 2004, *Phys. Rev. Lett.*, 93, 1301
223. Starobinsky A.A., 1993, *JETP Lett.*, 57, 622
224. Tegmark M., Eisenstein D.J., Hu W. & de Oliveira-Costa A., 2000, *ApJ*, 530, 133
225. Tegmark M., de Oliveria-Costa A., Hamilton A.J., 2003, *Phys. Rev. D*, 68, 123523
226. Tegmark M. et al., 2004, *ApJ*, 606, 702
227. Tegmark M. et al., 2004, *Phys. Rev. D*, 69, 103501
228. Tenorio L., Jaffe A.H., Hanany S., Lineweaver C.H., 1999, *MNRAS*, 310, 823
229. Tonry J.L. et al., 2003, *ApJ*, 594, 1

230. Tucci M., Martínez-González E., Vielva P. & Delabrouille J., 2005, MNRAS, 360, 935
231. Toffolatti L., Negrello M., González-Nuevo J., de Zotti G., Silva L., Granato G.L. & Argüeso F., 2005, A&A, 438, 475 astro-ph/0410605
232. Tojeiro R., Castro P.G., Heavens A.F. & Gupta S., 2006, MNRAS, 365, 265
233. Tomita K., 2005, Phys. Rev. D, 72, 103506
234. Turok N. & Spergel D., 1990, Phys. Rev. D, 64, 2736
235. Uzan, J.-P., Lehoucq, R. & J.-P. Luminet, J.-P. 1999. In *Proceedings of the XIXth Texas Symposium*, Paris 14-18 December 1998, Eds. E. Aubourg, T. Montmerle, J. Paul and P. Peter, article-no: 04/25
236. Vale C., 2005, ApJL, submitted, astro-ph/0509039
237. Vielva P., Barreiro R. B., Hobson M. P., Martínez-González E., Lasenby A. N., Sanz J. L. & Toffolatti L., 2001, MNRAS, 328, 1
238. Vielva P., Martínez-González E., Barreiro R.B., Sanz J.L. & Cayón L., 2004, ApJ, 609, 22
239. Vielva P., Martínez-González E. & Tucci M., 2006, MNRAS, 365, 891, astro-ph/0408252
240. Vilenkin A. & Shellard E.P.S., 1994, *Cosmic Strings and Other Topological Defects*, Cambridge University Press
241. Vishniac E.T., 1986, ApJ, 322, 597
242. Wandelt B.D., Hivon E. & Gorski K.M., 1998: Topological Analysis of High-Resolution CMB Maps. In: *Fundamental Parameters in Cosmology*, proceedings of the XXXIIIrd Rencontres de Moriond, ed. by Tran Thanh Van (Eds. Frontières 1998), astro-ph/9803317
243. Watson R.A., Rebolo R., Rubio-Martín J.A., Hildebrandt S., Gutiérrez C.M., Fernández-Cerezo S., Hoyland R.J. & Battistelli E.S., 2005, ApJ, 624, L89, astro-ph/0503714
244. Weeks, J. 1998, Class. Quant. Grav., 15, 2599
245. Weeks J.R., 2004, astro-ph/0412231
246. White N.E., 2005, Adv. Space Res., 35, 96
247. Wiaux Y., Jaques L. & Vandergheynst P., 2005, ApJ, submitted, astro-ph/0508516
248. Wiaux Y., Vielva P., Martínez-González E. & Vandergheynst P., 2006, Phys. Rev. Lett., 96, 151303
249. Wu J.H.P.: New Method of Extracting non-Gaussian Signals in the CMB. In: *20th Texas Symposium on relativistic astrophysics, Austin, Texas, 10-15 December, 2000*, vol. 586, ed. by J.C. Wheeler and H. Martel (AIP Conference Proceedings), p. 211
250. Wu, J.H.P., Balbi, A., Borriol, J., Ferreira, P.G., Hanany, S., Jaffe, A.H., Lee, A.T., Rabbii, B., Richards, P.L., Smoot, G.F., Stompor, R. & Winant, C.D. 2001, Phys. Rev. Lett., 87, 251303, astro-ph/0104248.
251. Wu, J.-H.P., 2005, astro-ph/0501239
252. Wyman M., Pogosian L. & Wasserman I., 2005, Phys. Rev. D, 72, 023513
253. Yoshida N., Sheth R. K. & Diaferio A., 2001, MNRAS, 328, 669, astro-ph/0104332
254. Zaldarriaga M. & Seljak U., 1997, Phys. Rev. D, 55, 1830
255. Zaldarriaga M. & Seljak U., 1998, Phys. Rev. D, 58, 023003